

1 **Humoral immune response to adenovirus induce tolerogenic**
2 **bystander dendritic cells that promote generation of regulatory T**
3 **cells**

4 Thi Thu Phuong Tran¹, Karsten Eichholz¹, Patrizia Amelio², Crystal Moyer³, Glen R
5 Nemerow³, Matthieu Perreau², Franck JD Mennechet¹ & Eric J Kremer¹

6 ¹Institut de Génétique Moléculaire de Montpellier, University of Montpellier, CNRS,
7 Montpellier, France

8 ²Division of Immunology & Allergy, University of Lausanne, Lausanne, Switzerland

9 ³Department of Immunology and Microbial Science the Scripps Research Institute, La
10 Jolla, CA, USA

11 **Short title:** IgG-complexed adenovirus and tolerance

12 **Keywords:** adenovirus; antibodies; tolerogenic dendritic cells; pyroptosis; innate
13 immunity; T_{regs}

14 **Correspondence:** eric.kremer@igmm.cnrs.fr

15 **Abstract**

16 Following repeated encounters with adenoviruses most of us develop robust humoral and
17 cellular immune responses that are thought to act together to combat ongoing and
18 subsequent infections. Yet in spite of robust immune responses, adenoviruses establish
19 subclinical persistent infections that can last for decades. While adenovirus persistence
20 pose minimal risk in B-cell compromised individuals, if T-cell immunity is severely
21 compromised, reactivation of latent adenoviruses can be life threatening. This dichotomy
22 led us to ask how anti-adenovirus antibodies influence adenovirus-specific T-cell
23 immunity. Using primary human blood cells, transcriptome and secretome profiling, and
24 pharmacological, biochemical, genetic, molecular, and cell biological approaches, we
25 initially found that healthy adults harbor adenovirus-specific regulatory T cells (T_{regs}). As
26 peripherally induced T_{regs} are generated by tolerogenic dendritic cells (DCs), we then
27 addressed how tolerogenic DCs could be created. Here, we demonstrate that DCs that
28 take up immunoglobulin-complexed (IC)-adenoviruses create an environment that causes
29 bystander DCs to become tolerogenic. These adenovirus antigen-loaded tolerogenic DCs
30 can drive naïve T cells to mature into adenovirus-specific T_{regs} . Our results may provide
31 ways to improve antiviral therapy and/or pre-screening high-risk individuals undergoing
32 immunosuppression.

33 **Author summary**

34 While numerous studies have addressed the cellular and humoral response to primary
35 virus encounters, relatively little is known about the interplay between persistent
36 infections, neutralizing antibodies, antigen-presenting cells, and the T-cell response. Our
37 studies suggests that if adenovirus–antibody complexes are taken up by professional
38 antigen-presenting cells (dendritic cells), the DCs generate an environment that causes
39 bystander dendritic cells to become tolerogenic. These tolerogenic dendritic cells favors
40 the creation of adenovirus-specific regulatory T cells. While this pathway likely favors
41 pathogen survival, there may be advantages for the host also.

42 Introduction

43 Human adenoviruses (HAdVs), of which there are currently >80 types, typically cause
44 self-limiting respiratory, ocular, and gastro-intestinal tract infections in immunocompetent
45 individuals. After repeated encounters, most young adults generally harbor cross-reactive,
46 long-lived humoral and T-cell responses [1–3] that are thought to work together to
47 efficiently blunt subsequent HAdV-induced morbidity. However, in spite of the robust anti-
48 HAdV immune responses, HAdVs routinely establish decades-long, subclinical infections
49 that are characterized by low level shedding of progeny virions [4,5]. While potential
50 molecular mechanisms by which HAdVs evade the immune response have been
51 proposed [6], we suspected that complementary mechanisms also exist. Of note, in T-cell
52 compromised patients the loss of cellular control of persistent HAdV infection can lead to
53 fulminant and fatal disease [4,5]. It is noteworthy that serological evidence that the patient
54 has been infected by a given HAdV type before hematopoietic stem cell transplantation is
55 predictive of escape from the same HAdV type during immune suppression [7].

56 While T-cell therapy has shown a notable potential to prevent HAdV disease in
57 immunocompromised patients [8,9], immunoglobulin therapy has had remarkably little
58 impact [4]. Due to omnipresent anti-HAdV antibodies, it is not surprising that
59 immunoglobulin-complexed HAdVs (IC-HAdVs) are detected in some patients with HAdV
60 disease [10–12]. In a broader view, immunoglobulin-complexed viruses can form during
61 prolonged viremia, secondary infections, primary infections when a cross-reactive humoral
62 response exists, and in the presence of antibody-based antiviral therapy. It is important to
63 note that IC-HAdVs are potent stimulators of human dendritic cell (DC) maturation [13,14].
64 In immunologically naïve hosts, immunoglobulin-complexed antigens are efficient
65 stimulators of antibody and cytotoxic T-cell responses [15]. However, most studies using
66 immunoglobulin-complexed antigens have used prototype antigens that have little impact
67 on their intracellular processing. This is not the case for IC-HAdVs. The endosomolytic
68 activity of protein VI, an internal capsid protein, prevents the canonical processing of the
69 IC-HAdVs by enabling the escape of HAdV capsid and its genome from endosomes into
70 the cytoplasm [14]. In the cytoplasm, the HAdV genomes are detected by absent in
71 melanoma 2 (AIM2), a cytosolic pattern recognition receptor (PRR) [16]. AIM2
72 engagement of the 36 kb HAdV-C5 genome induces pyroptosis, a pro-inflammatory cell
73 death in conventional DCs [17]. Pyroptosis entails inflammasome formation, caspase 1
74 recruitment/auto-cleavage/activation, pro-IL-1 β processing, gasdermin D (GSDMD)
75 cleavage, GSDMD-mediated loss of cell membrane integrity, and IL-1 β release [18,19].

76 Just as immune responses need to be initiated, suppression of cellular responses are
77 primordial to avoid excessive tissue damage and feature prominently in acute and chronic

78 infection [20–22]. Control of antigen-specific T cells can be mediated in part by
79 peripherally induced regulatory T cells (T_{regs}) [23]. When regulation of immune responses
80 goes awry, antigen-specific T_{regs} can favor the establishment of persistent viral infections.
81 Moreover, tolerogenic DCs are required for antigen-specific T_{reg} formation. The variable
82 phenotype and functionality of tolerogenic DCs are globally characterized by a semi-
83 mature profile encompassing cell surface costimulatory molecules, cytokine expression
84 and secretion, and antigen uptake and processing [24,25].

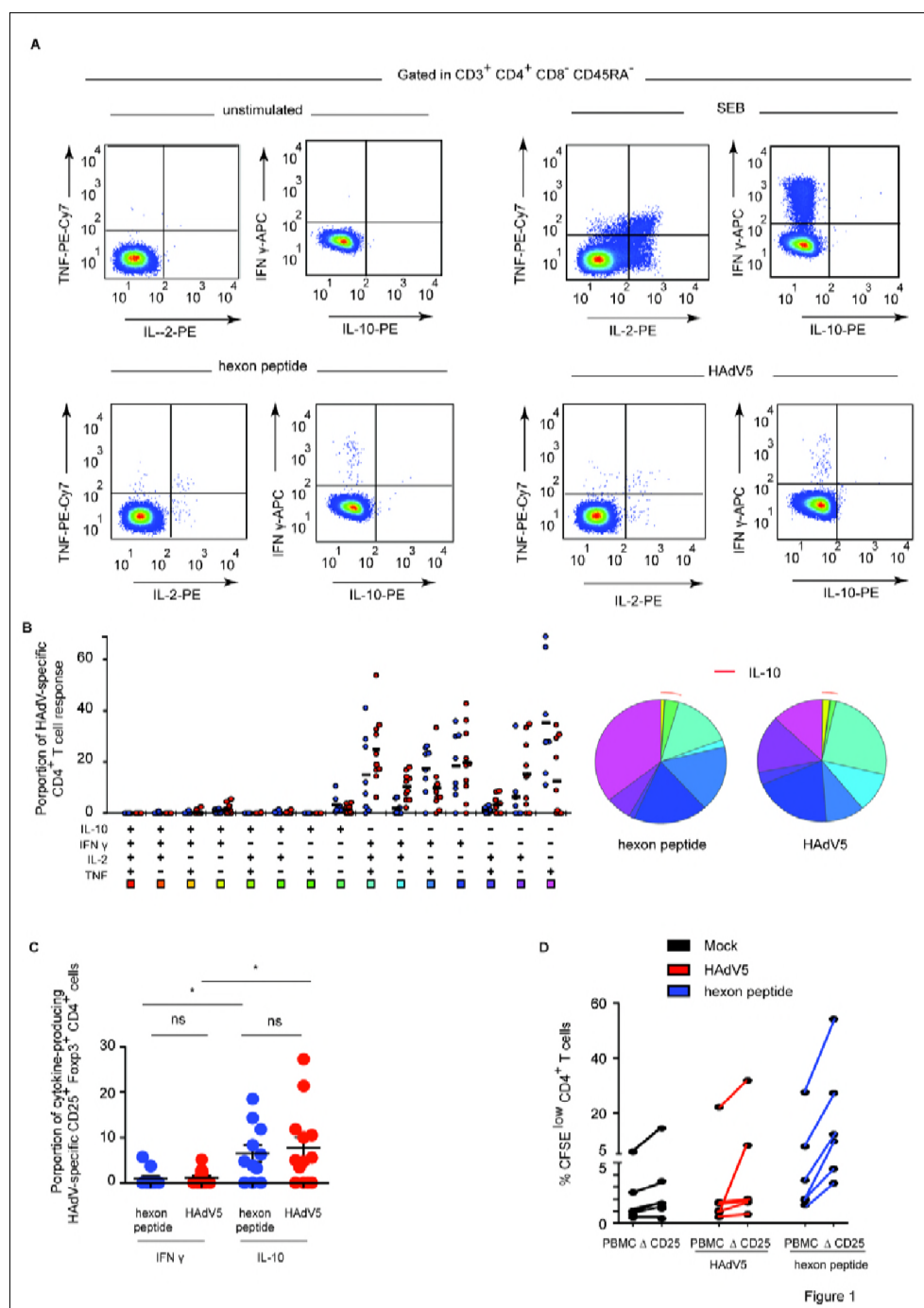
85 The goals of our studies were to determine how HAdV-specific humoral immunity impacts
86 the cellular response to HAdVs, and whether this might affect persistence. Initially, we
87 found that healthy adults harbor HAdV-specific T_{regs} . We then demonstrated that IC-
88 HAdV5-challenged human DCs induce a tolerogenic phenotype in bystander DCs. We
89 show that the bystander DCs are capable of taking up and presenting HAdV antigens, and
90 can drive naïve T cells to mature into HAdV-specific T_{regs} . Our study reveals a mechanism
91 by which an antiviral humoral responses could, counterintuitively, favor virus persistence.

92 Results

93 HAdV-specific T_{regs} in healthy donors dampen HAdV-specific T cell proliferation

94 Initially, we asked if healthy adults harbor HAdV-specific T_{regs} and if so, are they capable
95 of dampening HAdV-specific T-cell proliferation. To address these questions, we pre-
96 screened a cohort of healthy individuals using an IFN- γ ELISpot assay for a memory T-cell
97 response to HAdV5 using a pool of overlapping hexon peptides (hexon is the major
98 protein in the HAdV capsid). PBMCs from individuals with a spot forming unit ratio 5-fold
99 greater than mock-treated cells were selected for further analyses. Because inducible T_{regs}
100 can produce IL-10 in response to their cognate antigen, the ability of HAdV-specific CD4⁺
101 T cells to produce IL-10 as well as IFN- γ , TNF, and IL-2 was assessed by multi-parametric
102 flow cytometry. Consistent with our previous results [13], the cytokine profile of HAdV-
103 specific memory CD4⁺ T cells was dominated by polyfunctional IFN- γ ⁺/IL-2⁺/TNF⁺/IL-10⁻
104 cells (approximately 25% of total HAdV-specific CD4⁺ T cells) and IFN- γ ⁺/IL-2⁻/TNF⁻/IL-10⁻
105 cells (approximately 20%) (**Figure 1A**, a representative donor). We then characterized the
106 combinations of the responses and the percentage of functionally distinct populations in
107 all donors (**Figure 1B**). Each slice of the pie chart corresponds to HAdV-specific CD4⁺ T
108 cells with a given number of functions, within the responding T-cell population. Of note, IL-
109 10-producing HAdV-specific CD4⁺ T cells, which were approximately 5% of total, were
110 predominantly IFN- γ ⁻/IL-2⁻/TNF⁻. To determine if the IL-10 producing T cells have a T_{reg}
111 phenotype, the expression of conventional T_{reg} markers, CD45RO, CD25, FoxP3, and
112 CD127 [26], were assessed. We found that approximately 8% of the IL-10 producing T
113 cells were CD25⁺/FoxP3⁺/CD127^{dim}. By contrast, most of IFN- γ producing HAdV-specific
114 CD4⁺ T cells harbored a conventional memory phenotype (CD45RO⁺/FoxP3⁻/CD25⁻
115 /CD127⁺) (**Figure 1C**). These data demonstrate the presence of HAdV-specific T_{regs} in
116 healthy adults.

117 To determine if putative HAdV-specific T_{regs} have regulatory functions, we incubated
118 CFSE-labeled PBMCs, or PBMCs depleted in CD25-expressing cells, with a hexon
119 peptide pool and quantified T-cell proliferation. We found that depletion of all CD25⁺ cells
120 caused CD4⁺ cells to proliferate greater than control peptide-challenged CD4⁺ cells
121 (**Figure 1D**), suggesting that the HAdV-specific T_{regs} in the CD25⁺ population can restrict
122 the proliferative anti-HAdV-specific T cells. Taken together, these data indicate that a
123 fraction of HAdV-specific CD4⁺ T cells harbors an inducible T_{reg} phenotype, and that
124 healthy adults have T_{regs} that dampen the proliferation of HAdV-specific T cells.



125

126 **Figure 1) HAdV-specific T_{regs} are present in normal healthy adults**

127 **A)** Representative flow cytometry profile of hexon peptides- and HAdV5-specific (bottom left and right panels)
 128 CD4 T cells producing TNF, IL-2, IFN- γ , and IL-10 in a representative subject. Top left panel: mock stimulated
 129 (negative control). Top right panel: cytokine profiles of CD4 T cells stimulated with SEB (Staphylococcal
 130 enterotoxin B, positive control). **B)** Cumulative (n = 11 donors) cytokine profiles of hexon peptides (blue
 131 points) and HAdV5 (red points) CD4 T cells producing TNF, IL-2, IFN- γ , and IL-10. All possible combinations
 132 of responses are shown on the x-axis, and the percentage of functionally distinct cell populations within the
 133 CD4 T-cell populations are shown on the y-axis. Responses are grouped and color-coded on the basis of the
 134 number of functions. The pie chart summarizes the data, and each slice corresponds to the fraction of CD4 T
 135 cells with a given number of functions, within the responding CD4 T cells. Red arcs correspond to IL-10
 136 producing CD4 T cell. **C)** Proportion of IL-10 or IFN- γ -producing HAdV5-specific CD4 T cells expressing CD25
 137 and FoxP3 among IL-10, or IFN- γ , producing HAdV5-specific CD4 T cells. **D)** Proliferation of CFSE-labeled
 138 PBMCs and PBMCs depleted in CD25⁺ cells (Δ CD25) activated by HAdV5 (red lines) or hexon peptides (blue
 139 lines) and cultured for 7 days. The cells were analyzed by flow cytometry for proliferation (CFSE^{low}) and CD4
 140 using FlowJo software (n = 6 donors and assayed in duplicate).

141 **Phenotypic maturation of bystander DCs**

142 A prerequisite for antigen-specific T_{reg} formation is the presence of antigen-presenting
143 tolerogenic DCs [27,28]. Because the cellular profile of HAdV5-challenged DC [29] is
144 inconsistent with that of tolerogenic DCs [29], we asked if IC-HAdV5 could be involved in
145 the generation of HAdV-presenting tolerogenic DCs. When HAdV5 is mixed with
146 neutralizing antibodies from human sera, 200 nm-diameter complexes are formed that
147 induce DCs to undergo pyroptosis, or, if the DC does not die, a hypermature profile
148 [13,14]. As these profiles are also inconsistent with that of tolerogenic DCs, we
149 hypothesized that it was not due to IC-activated DCs, but rather an effect on bystander
150 DCs.

151 To assess the impact of IC-HAdV5-induced pyroptosis and DC maturation on bystander
152 DCs we developed a transwell assay (**Figure S1A** for schematic). Briefly, CD14⁺
153 monocytes isolated from fresh buffy coats were induced to differentiate into immature DCs
154 for 6 days. Immature DCs seeded in 12-well plates were mock-treated, challenged with
155 bacterial lipopolysaccharides (LPS), HAdV5, IgGs, or IC-HAdV5 (these cells will be
156 referred to “direct DCs”). At 6 h post-challenge, a transwell insert was added and naive
157 immature DCs (bystander DCs) from the same donor were seeded in the upper chamber
158 (see **Figure S1B-D** for controls concerning transfer of HAdV5 particles between chambers
159 and cell death). Twelve hours after adding the bystander DCs to the upper chamber, the
160 direct and bystander DCs were collected and assayed as described below. Compared to
161 bystander DCs stimulated by direct DCs challenged with IgG or HAdV5, bystander DCs
162 stimulated by IC-HAdV5-challenged DCs increased their cell surface levels of the
163 maturation/activation markers CD80, CD83, CD86 (**Figure 2A**), CD40, and MHC II
164 (**Figure S2A**). The level of CD86 on bystander DCs tended to increase as the number of
165 IC-HAdV5 particles increased during the stimulation of the direct DCs (**Figure S2B**). The
166 cell surface increase of CD86 and CD83 was also accompanied by an increase in total
167 (cell surface + intracellular) CD86 and CD83 levels (**Figure 2B**). Together, these data
168 demonstrate that IC-HAdV5-challenged DCs enhanced the synthesis and cell surface
169 expression of maturation/activation markers on bystander DCs.

170
171
172
173
174
175
176
177
178
179
180
181
182
183
184
185
186
187
188
189
190
191
192
193
194
195
196
197
198
199
200
201

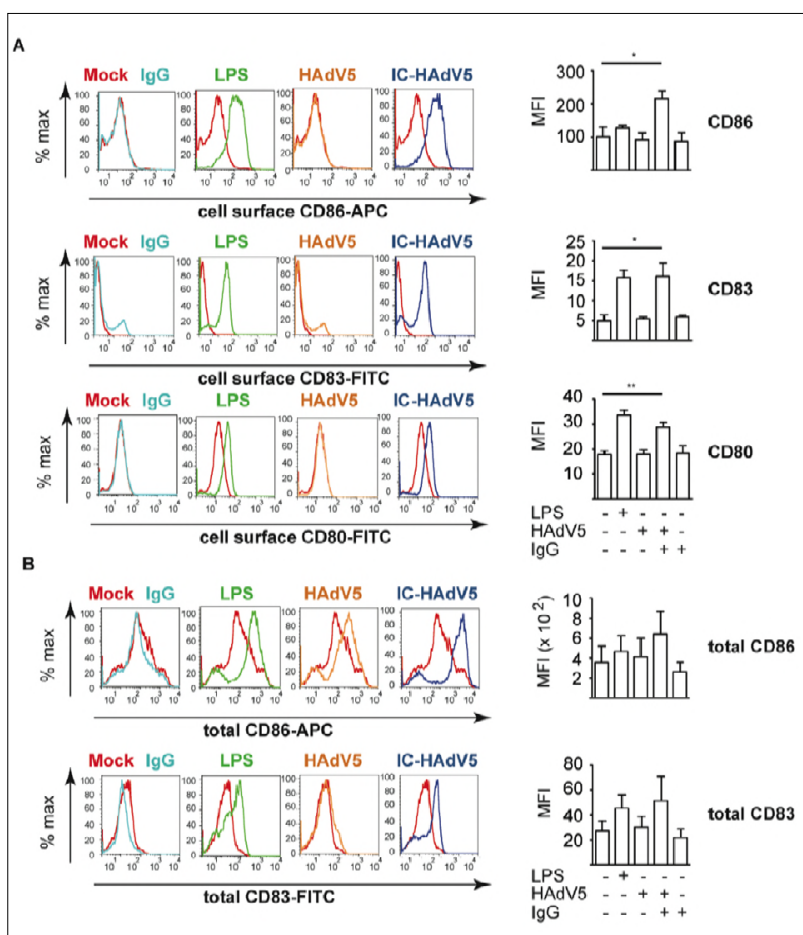
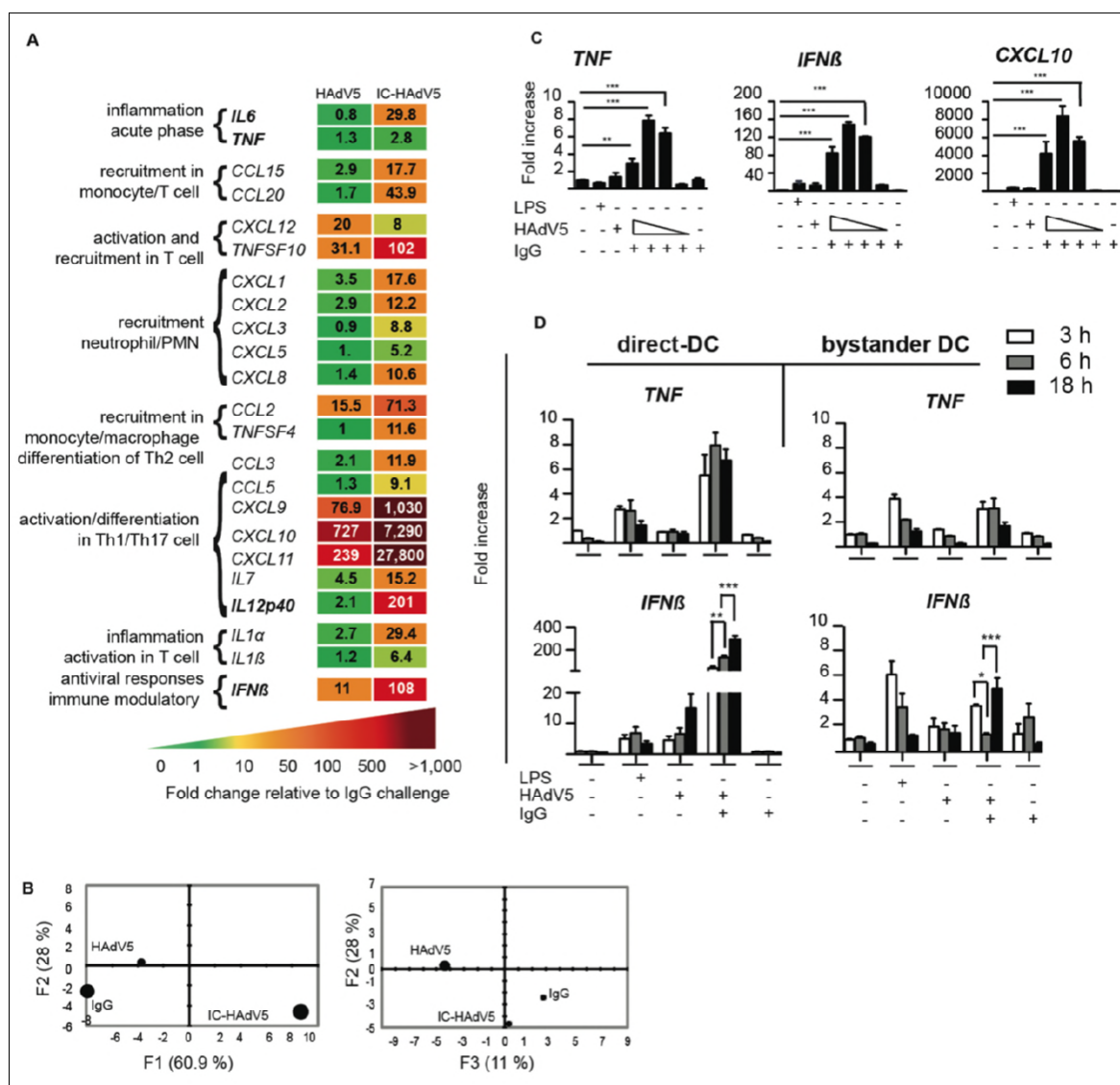


Figure 2) Activation/maturation marker expression in bystander DCs

Representative flow cytometry profile of cells that were mock-treated (red), challenged with IgG (light blue), LPS (green), HAAdV5 (orange), or IC-HAdV5 (dark blue). **A**) The cell surface expression of CD86 (top panels), CD83 (middle panels), and CD80 (bottom panels) were quantified 12 h post-stimulation. The profile of mock-treated cells is included in each panel as a reference. Assays were carried out in duplicate in 5 donors with similar results. **B**) Representative flow cytometry profile of total (intracellular and extracellular) CD86 and CD83 levels in bystander DCs incubated with DCs challenged with IgG, LPS, HAAdV5, or IC-HAdV5 12 h post-stimulation (color-coded as in **A**). The mock-treated cells are included in each panel as references. The graphs to the right are the cumulative data from 4 donors and performed in duplicate. Error bars are \pm SEM. * $p < 0.05$, ** $p < 0.01$.

202 The cytokine transcriptome of bystander DCs suggests a tolerogenic profile

203 To characterize bystander DC functional capabilities we used an 84-plex inflammatory
204 cytokine, chemokine and their receptor mRNA array to quantify transcriptional changes
205 (**Figure S2C** for the list of mRNAs that gave unique amplification profiles). Stimulation of
206 bystander DCs with the milieu from HAAdV5-challenged DCs (without IgGs) led to notable
207 increases (>50 fold) in mRNA levels of Th1/Th17 cell activation/differentiation markers
208 (e.g. *CXCL9*, *CXC10* & *CXC11*) (see **Figure S2C** for all data and **Figure 3A** left hand
209 columns for selected data). By contrast, the bystander DC response to the IC-HAdV5-
210 challenged DCs was greater with respect to the number of mRNAs altered (>20) and
211 magnitude (up to 10,000-fold increase) (**Figure 3A** right column, and **Figure S2C** middle
212 column). Of particular relevance was the lack of *TNF* mRNA by bystander DC because
213 tolerogenic DCs should not, *a priori*, secrete TNF. To better understand the transcriptional
214 responses of the different conditions, we applied a principal component analysis (PCA) to
215 find patterns in these data sets. We found that two principal components (see **Materials &**
216 **Methods** for genes in the F1, F2, and F3 axes) explained 89% and 39% of the total
217 information, respectively, and each stimulus is distinguishable from the others (**Figure**
218 **3B**).



219

220 **Figure 3) Bystander DC cytokine transcription profile**

221 **A)** Transcription profile of selected cytokines from bystander DCs at 12 h post-activation following exposure to
 222 HAdV5- or IC-HAdV5-challenged direct DCs. The transcription profile of bystander DCs created by IgG-
 223 challenged direct DCs was used as the baseline. For the genes in bold, primer sequences were designed in-
 224 house (n = 2 donors). **B)** Principal component analysis (PCA) of the changes in the 66 mRNAs included in the
 225 array. Three principal components showed 61% (F1), 28% (F2), and 11% (F3) accordance. **C)** *TNF*, *IFN β* ,
 226 and *CXCL10* mRNA levels in bystander DCs. Direct DCs were mock-, IgG-, LPS-, HAdV5-, or IC-HAdV-
 227 challenged. IC-HAdV5s were used at 20 x 10³, 10 x 10³, 5 x 10³, or 1 x 10³ physical particles/direct DC.
 228 Assays were carried out in 3 donors in at least duplicates. The fold increase is shown as mean \pm SEM. See
 229 **Table S1** for additional statistical analyses. **D)** Kinetics (3, 6, 18 h) of *TNF* (top panels) and *IFN β* (bottom
 230 panels) mRNA levels of THP-1-derived DC challenged with LPS, HAd5, IgG or IC-HAdV5 (left panels) or
 231 bystander DCs (using the milieu from the direct DCs in the left panel) (right panels). Three independent
 232 assays in duplicate were performed. The fold increase is shown as the mean \pm SEM. *P* values were derived
 233 from one-way ANOVA with Dunnett's test: ** *p* < 0.01 and *** *p* < 0.001.

234 Because a cell infected by one HAdV particle could produce >10⁴ virions ~36 h later, local
 235 and global HAdV levels, as well as IC-HAdV formation, are dynamic. Of note, IC-HAdV5
 236 causes a dose-dependent induction of pyroptosis in direct DCs [14]. We therefore
 237 extended the mRNA array analyses by quantifying dose-dependent response of bystander
 238 DCs. Using RT-qPCR we analyzed *TNF*, *IFN β* and *CXCL10* (**Figure 3C**) and *IL1 β* , *IL12*

239 (p40), *CCL3* and *IL6* (**Figure S2D**) mRNA levels. In all cases the transcriptional response
240 of bystander DCs varied depending on the IC-HAdV5 challenge dose. These data suggest
241 that the bystander DC response is linked to the percentage of direct DCs undergoing
242 pyroptosis [14].

243 To characterize time-dependent transcriptional changes in direct DC and bystander DCs,
244 we compared mRNA levels of *TNF*, *IFN β* (**Figure 3D**), *Mip-1 α* and *IL6* (**Figure S3**, which
245 also includes dose-dependent response). Globally, mRNAs that code for pro-inflammatory
246 molecules were 2 to 10-fold greater in direct DCs than in bystander DCs. In addition, only
247 *IL1 β* and *Mip-1 α* mRNA levels changed significantly ($p < 0.01$) over time. These data
248 demonstrate that bystander DCs have a semi-mature tolerogenic transcriptional profile,
249 which is linked to DC pyroptosis, and lack noteworthy levels of *TNF* mRNA [30].

250 **Cytokine secretion by bystander DCs is consistent with a tolerogenic profile**

251 To examine the events downstream the transcriptional response, we quantified the
252 secreted cytokine from direct and bystander DCs. Because proteins can readily diffuse
253 across the transwell membranes, bystander DCs were removed from the upper chamber
254 12 h post-challenge, rinsed, and then placed in a separate well with fresh medium for 9 h
255 before collecting the medium. The direct DC medium was collected at 12 h post-
256 challenge, or after a wash at 12 h and then collected 9 h later (21 h) to compare
257 conditions similar to that used for bystander DCs (see **Figure 4A** for schematic).
258 Challenging DCs with HAdV5 alone had a modest effect on their secretome with the
259 exception of a 5 to 10-fold increase in TNFSF10, and CXCL9 & 10 levels (**Figure 4B**,
260 second column from the left). By contrast, IC-HAdV5-challenged DCs responded with
261 increases of >15 fold in approximately half of the cytokines (**Figure 4B**, middle columns).
262 These data are consistent with previous results showing the robust maturation of IC-
263 HAdV5-challenged DCs [13,14]. HAdV5-challenge DCs that were rinsed 12 h post-
264 stimulation had overall lower cytokine levels than prior to washing, but TNFSF10, CXCL9,
265 CXCL11, and CCL5 levels remained robust (**Figure 4C**, middle columns). Interestingly,
266 instead of a positive correlation between the cytokine secretion and the IC-HAdV5 dose,
267 we found that as the IC-HAdV5 dose increased, the cytokines secreted by direct DCs
268 tended to decrease (**Figure 4C**, middle columns).

269 Using HAdV5-challenged DCs (without IgGs) to generate bystander DCs, we found that
270 the latter secreted 3 to 12-fold higher levels of TNFSF10, CCL5, CXCL9, CXCL10 and
271 CXCL11 compared to bystander DCs exposed to the medium from IgG-challenged DCs
272 (**Figure 4D**, second column). Similarly, when bystander DCs were generated using IC-
273 HAdV5-challenged DCs, the level of the above five cytokines also increased. In addition,

274 three chemokines involved in immune cell recruitment (CCL15, CCL20, and CCL2)
 275 increased >3 fold. Consistent with the transcriptome analyses, we did not find a notable
 276 dose-dependent effect on bystander DCs when direct DCs were incubated with increasing
 277 IC-HAdV5 particles (**Figure 4D**, middle columns).



Figure 4) Direct and bystander DC cytokine secretomes

320 Together, these data suggest that the release of pathogen-associated molecular patterns
 321 (PAMPs), danger-associated molecular patterns (DAMPs), and/or the increased levels of
 322 cytokines secreted by a greater number of DCs that do not undergo pyroptosis, are key
 323 factors in bystander DC maturation. In addition, the environment created by IC-HAdV5
 324 induces a semi-mature cytokine secretion profile in bystander DCs.

325 Cytokines and pyroptosis-associated factors impact bystander DC phenotype

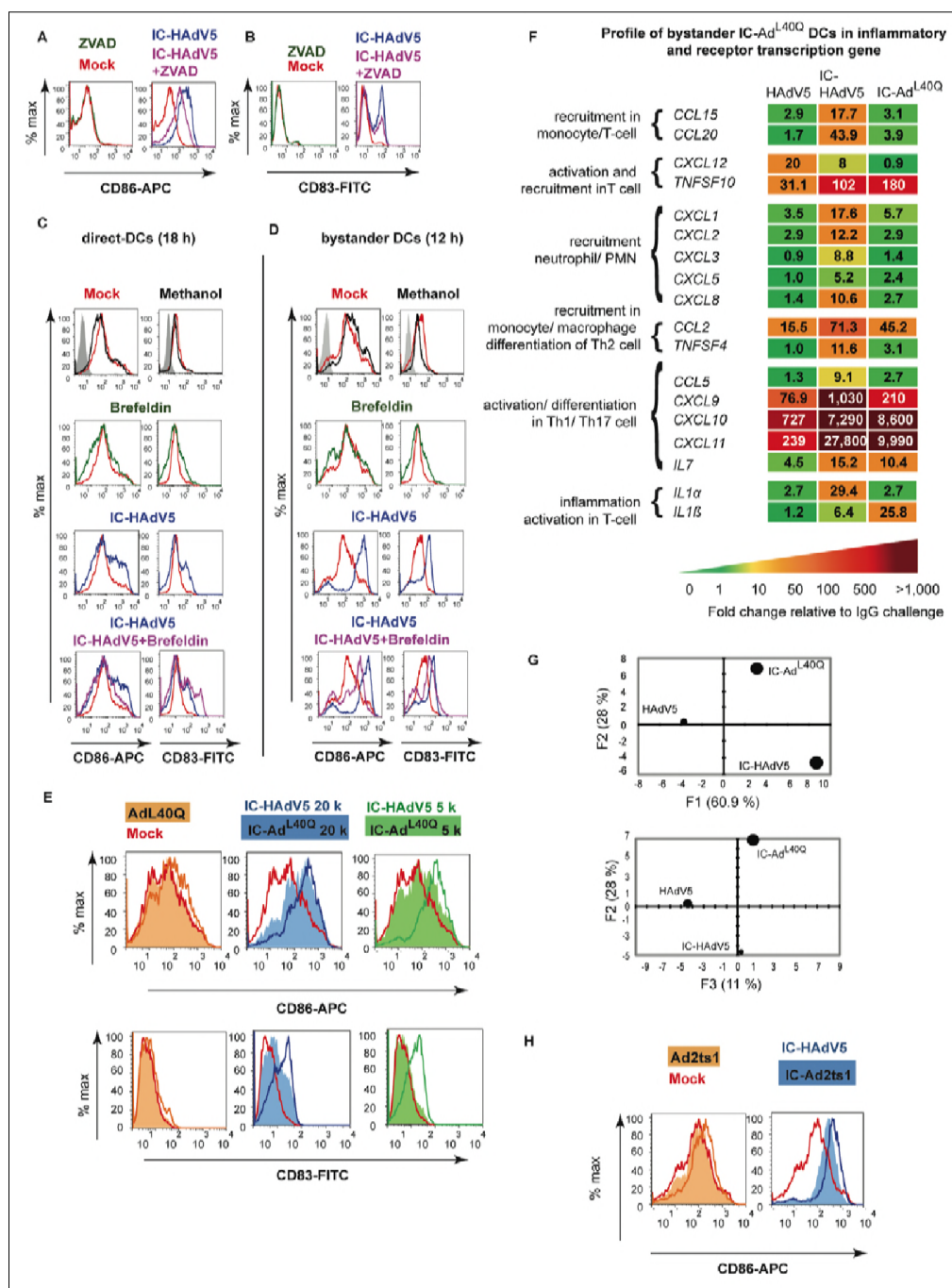
326 To determine how cytokines and pyroptosis impact bystander DCs, we used a
327 combination of drugs and mutant viruses to selectively modify the environment created by
328 IC-HAdV5-challenged DCs. To determine the impact of IL-1 β , direct DCs were pre-treated
329 with ZVAD, a pan-caspase inhibitor that blocks caspase 1 auto-cleavage and pro-IL-1 β
330 processing. Importantly, ZVAD has no effect on TNF and canonical protein secretion
331 (**Figure S4A** and reference [14]). We found that blocking IL-1 β production by direct DCs
332 reduced bystander DC maturation as demonstrated by their lower levels of CD86 and
333 CD83 (**Figure 5A-B**). We then used brefeldin A to block ER to Golgi-mediated cytokine
334 secretion in direct DCs (see **Figure S4B** for controls). Of note IL-1 β release is not
335 significantly affected by brefeldin A, (**Figure S4C**). In brefeldin A-treated IC-HAdV5-
336 challenged DCs the levels of CD83 and CD86 did not change markedly (**Figure 5C**), while
337 the bystander DCs responded with lower levels of CD83 and CD86 (**Figure 5D**).

338 Next, we generated ICs using Ad^{L40Q} [31], an HAdV5 capsid containing a mutated protein
339 VI that attenuates endosomolysis. While IC-Ad^{L40Q} poorly induces pyroptosis in direct DCs
340 [14], they secrete levels of TNF that are similar to IC-HAdV5-challenged DCs.
341 Furthermore, *IFN β* and *IL1 β* mRNA levels are lower [14]. We found notably lower levels of
342 CD86 and CD83 on bystander DCs following stimulation with the response from IC-
343 HAdV5 versus IC-Ad^{L40Q}-challenged DCs. In addition, the reduced maturation/activation
344 effects were only modestly altered by increasing the IC-Ad^{L40Q} dose (**Figure 5E**).
345 Together, these data demonstrate a role for pyroptosis-associated factors in the
346 maturation of bystander DCs.

347 We then compared cytokine mRNA levels in bystander DCs stimulated by HAdV5-, IC-
348 Ad^{L40Q}-, or IC-HAdV5-challenged DCs (**Figure 5F** and **Figure S5A-C**). Consistent with the
349 phenotype, the transcriptional responses of bystander DCs to both ICs were globally
350 higher than to HAdV5 alone. The bystander DC transcriptional response to IC-Ad^{L40Q}-
351 challenged DC milieu was generally lower than in IC-HAdV5-challenged DCs, and it was
352 qualitatively distinguishable as determined by PCA (**Figure 5G**).

353 We then assessed the effect of pyroptosis using IC-Ad2ts1. Ad2ts1 has a hyper-stable
354 capsid due to a mutation in protease that results in failure to process the capsid pre-
355 protein [32,33]. We previously showed that IC-Ad2ts1 poorly induces DC pyroptosis, likely
356 because the HAdV genome does not escape from the capsid and therefore does not
357 nucleate AIM2 (see reference [14] and **Figure S5D-F** for Ad2ts1 controls). Of note, TNF
358 levels are comparable in DCs challenged with IC-Ad2ts1 or IC-HAdV5 [14]. Here, we
359 found that IC-Ad2ts1-challenged DC induced an increase of CD86 cell surface levels on
360 bystander DCs (**Figure 5H**). Together, these data demonstrate that cytokines and

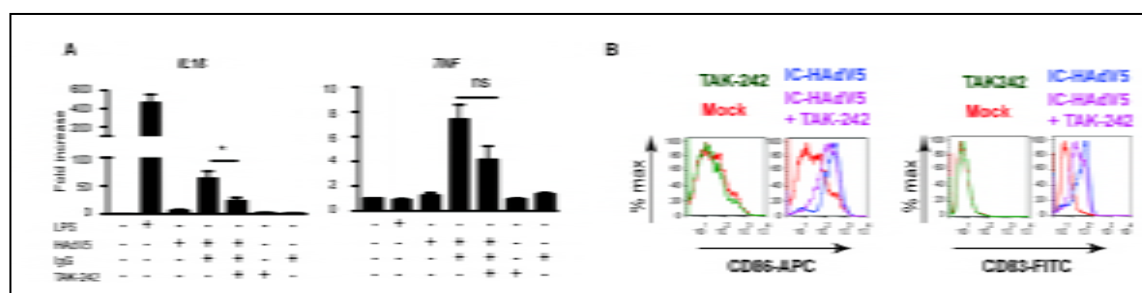
361 pyroptosis-associated factors play a role in the activation and semi-maturation of
 362 bystander DCs.



363
 364 **Figure 5) Impact of cytokines and pyroptosis-associated factors on bystander DC maturation**
 365 **A & B)** Shown are representative flow cytometry profile of direct DCs pretreated with ZVAD using the approach
 366 described in **Figure S1**. The cell surface levels of CD86 and CD83 on bystander DCs was quantified by flow
 367 cytometry ($n \geq 3$ donors). **C & D)** Representative flow cytometry profile of IC-HAdV5-challenged DCs treated with
 368 brefeldin A and the cell surface levels of CD86 and CD83 quantified by flow cytometry in direct DCs and
 369 bystander DCs ($n \geq 5$ donors). **E)** Bystander DCs were incubated with milieu generated by DC challenged with
 370 increasing doses of IC-Ad^{L40Q} (representative flow cytometry profiles of CD86 and CD83 levels). **F)** Bystander
 371 DC inflammatory cytokine mRNA levels were measured by RT-qPCR array following incubation with DC
 372 challenged with HAdV5, IC-HAdV5 and IC-Ad^{L40Q}. The heat map denotes the fold change relative to DCs
 373 challenged by IgGs ($n = 3$ donors). **G)** PCA of the changes in the 66 mRNAs included in the array when
 374 including IC-Ad^{L40Q}. **H)** Bystander DCs were incubated with milieu generated by DCs challenged with increasing
 375 doses of IC-Ad2ts1. Representative flow cytometry profiles of cell surface level of CD86 ($n = 2$ donors).

376 Engagement of TLR4 on bystander DCs

377 To characterize how bystander DCs are activated, we focused on Toll-like receptor 4
378 (TLR4). TLR4 is a multifunctional cell surface PRR that can directly or indirectly (by
379 forming a complex with MD-2, CD14, or other PRRs) be activated by extracellular viral
380 components (PAMPs) and, under inflammatory conditions, extracellular high-mobility
381 group box 1 and heat shock proteins (DAMPs) [34–36]. Of note, MD-2 acts as a co-
382 receptor for recognition of both exogenous and endogenous ligands [37–40]. While TLR4
383 does not bind to, or become activated by, HAdV5 alone [41], TLR4 might be activated by
384 PAMPs or DAMPs that interact directly with the HAdV5 capsid. We therefore used TAK-
385 242 to disrupt TLR4 signaling in bystander DCs (see **Figure S6** for TAK-242 control). As
386 readouts, we used the upregulation of *TNF* and *IL1 β* mRNAs, and activation/maturation
387 cell surface markers. When TLR4 signaling was blocked in bystander DCs stimulated by
388 the IC-HAdV5-challenged DC milieu, there was a significant ($p < 0.05$) decrease in *IL1 β*
389 mRNA levels and 2-fold decrease of *TNF* mRNA (**Figure 6A**). CD83 and, to a lesser
390 extent, CD86 levels were also reduced (**Figure 6B**). These data suggest that bystander
391 DCs use TLR4 to detect PAMPs and DAMPs released by IC-HAdV5-challenged DCs,
392 leading to changes in bystander DC maturation.



393
394 **Figure 6) Impact of TLR4 engagement on cytokine transcription and activation/maturation markers in**
395 **bystander DCs**

396 Involvement of TLR4 signaling in bystander DCs was assessed by **A)** *IL1 β* and *TNF* mRNA levels in
397 bystander DCs pre-treated with TAK-242, and then added to milieu of DCs challenged with LPS, IgG, HAdV5
398 and IC-HAdV5. Fold increase is represented as mean \pm SEM ($n = 3$ donors, * denotes $p < 0.05$) **B)**
399 Representative flow cytometry profiles of CD86 and CD83 cell surface levels in bystander DCs. DCs were
400 mock-treated (red line), TAK-242 alone (with TAK-242 and without direct DCs, green line) challenged with IC-
401 HAdV5 (dark blue) or pretreated with TAK-242 and challenged with the milieu generated from IC-HAdV5-
402 challenged DCs (violet line).

403 Minimal loss of phagocytosis in bystander DCs is consistent with tolerogenic 404 profile

405 Immature DCs survey the extracellular environment by random phagocytosis. Once PRRs
406 are engaged, DC maturation is accompanied by decreased uptake of fluid phase
407 molecules [42]. Of note, a functional hallmark of tolerogenic DCs is their ability to retain
408 some antigen uptake properties. To address the functional maturation of IC-HAdV5-

409 challenged DCs and bystander DCs, we incubated cells with FITC-labeled dextran and
410 quantified uptake by flow cytometry. We found that phagocytosis was modestly
411 downregulated in direct DCs stimulated with HAdV5 or LPS (**Figure 7A**). By contrast, IC-
412 HAdV5-challenged DC phagocytosis was near background levels, consistent with
413 complete maturation (see **Figure S7** for controls) [29]. While bystander DCs had reduced
414 phagocytosis when created by IC-HAdV5-challenged DCs, the bystander DCs still took up
415 17-fold more FITC-dextran than background levels (**Figure 7B**). These functional data are
416 consistent with semi-mature, tolerogenic DCs.

417

418

419

420

421

422

423

424

425

426

427

428

429

430

431

432

433

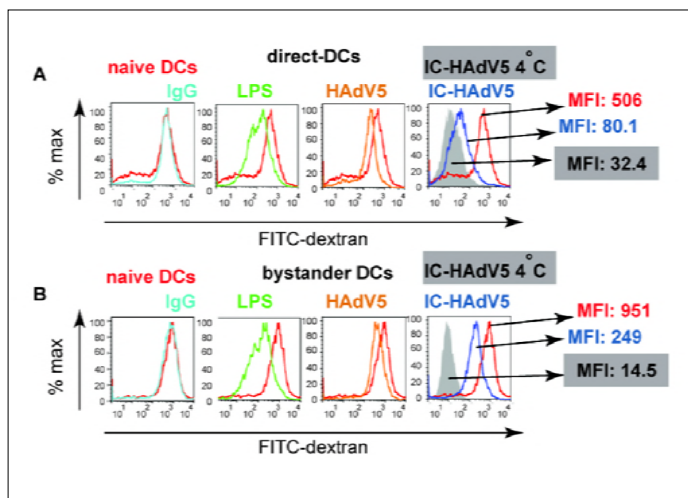


Figure 7) Fluid phase uptake by direct and bystander DCs

Fluid phase antigen uptake by direct and bystander DCs was quantified using FITC-labeled dextran and flow cytometry.

A) Representative flow cytometry profiles of direct DCs challenged with LPS,

HAdV5, IgG, or IC-HAdV5 and **B)**

Representative flow cytometry profiles of bystander DCs with the corresponding

direct DC milieu. Experiments were

performed 3 times, in duplicate, with

similar results. Nonspecific binding of

dextran to cells was controlled by

incubation at 4°C (**Figure S7**). MFI –

median fluorescent index.

434

435 **Bystander DCs create loop to recruit antigen-presenting cells**

436 While tolerogenic DCs can induce, recruit, and maintain T_{reg} homeostasis, tolerogenic

437 DCs can also create a feedback loop to promote their own generation [43]. Because

438 monocytes are recruited to sites of inflammation [44,45], we compared the functional

439 recruitment capabilities of direct DCs and bystander DCs (see **Figure S8** for setup and

440 controls). Unexpectedly, we found that IC-HAdV5-challenged DCs inhibited monocyte

441 recruitment in an IC-HAdV5 dose-dependent manner (**Figure 8A & B**). Of note, the

442 inhibition was abrogated when the IC-HAdV5-challenged DC were washed, suggesting

443 that inhibitory factors were generated <3 h post-IC-HAdV5 challenge (**Figure 8B**). To

444 determine if pyroptosis-related factors are responsible for the inhibition of monocyte

445 recruitment, we used IC-Ad^{L40Q} and ZVAD to reduce pyroptosis and IL-1 β secretion. The

446 effect of ZVAD was modest and did not markedly influence the monocyte recruitment

447 induced by IC-HAdV5-challenged DC, suggesting that pyroptosis related factors (e.g. IL-

448 1 β) did not have a role in this process (**Figure 8C & D**). In contrast to the IC-HAdV5-

449 challenged DC response, the IC-Ad^{L40Q}-challenged DC response significantly ($p < 0.05$)

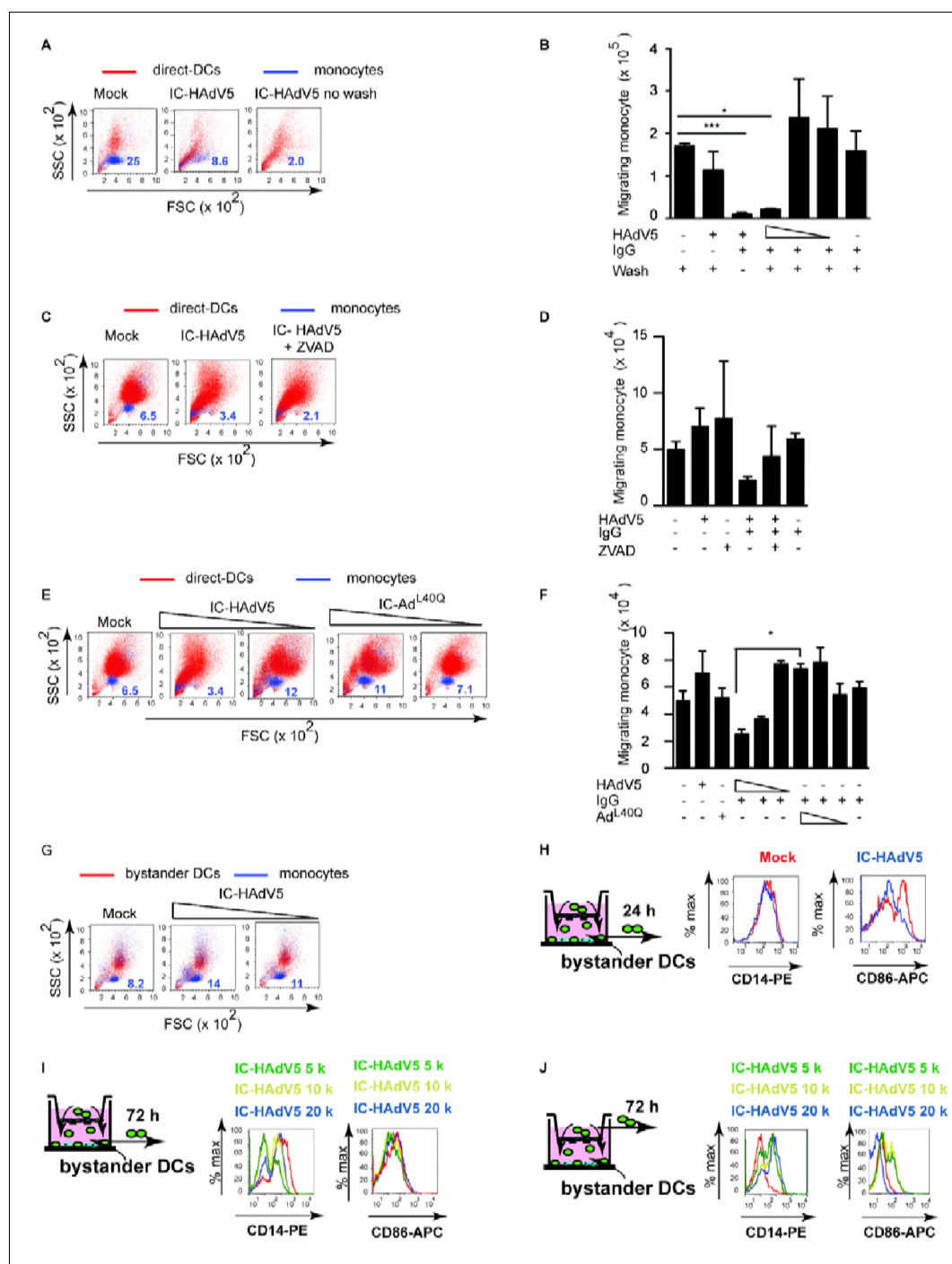
450 increased monocyte recruitment, in an IC-Ad^{L40Q} dose-dependent manner (**Figure 8E &**

451 **F**). These data demonstrate that pyroptosis factors other than IL-1 β inhibit monocyte

452 recruitment. We then examined the ability of bystander DCs to recruit monocytes. In
453 contrast to IC-HAdV5-challenged DCs, bystander DCs promoted monocyte recruitment
454 (**Figure 8G**). These data are consistent with the bystander DC milieu containing more
455 chemoattractants (**Figure 5**). There was also a trend towards greater recruitment when
456 higher IC-HAdV5 doses were used on the direct DCs.

457 Once monocytes migrate into an inflammatory environment they acquire distinct
458 phenotypic and functional profiles [46]. One phenotypic hallmark of monocyte
459 differentiation is CD14, which is high on monocytes and macrophages, but lower on DCs.
460 We therefore characterized migrating and static monocytes for CD14 and CD86 levels at
461 24 and 72 h (see schematic at the left of each panel in **Figure 8H-J** for the times and
462 location of cells, and **Figure S8** for controls). At 24 h the level of CD14 on monocytes that
463 had migrated into the bystander DCs environment did not change markedly, while CD86
464 levels were lower (**Figure 8H**). At 72 h the recruited monocytes had two distinct
465 populations based on CD14 levels (**Figure 8I**). The decrease in CD14 levels suggested
466 that they differentiated into DCs, while the CD86 levels suggest the maintenance of an
467 immature phenotype. In addition, monocytes recruited by bystander DCs had increased
468 CD14 levels. By contrast, CD86 levels decreased on monocytes in the upper chamber
469 (bottom chamber containing bystander DCs) (**Figure 8J**).

470 Together, these data demonstrate that DCs challenged with IC-HAdV5 inhibit monocyte
471 recruitment. Monocytes recruited to the bystander DC environment was abetted by
472 pyroptosis of direct DCs. Recruited monocytes had reduced CD14 levels, possibly due the
473 engagement and internalization of TLR4/CD14 complexes. Monocyte-DC contact also
474 appeared to favor the increase in cell surface levels of activation/maturation markers. We
475 concluded that the dynamic environment created by bystander DCs is consistent with a
476 feed-forward loop to foster tolerogenic DCs.



477

478

479

480

481

482

483

484

485

486

487

488

489

490

491

492

Figure 8) Direct and bystander DC monocyte recruitment and their phenotype

A 5 μ -pore transwell system (see **Figure S8** for details) was used for monocyte migration assays.

A) Representative FCS/SSC profiles of CFSE-labeled monocyte (blue) that migrated into the lower direct DC chamber; The numbers in dark blue correspond to the percentage of CFSE-labeled monocytes. **B)** Cumulative data from monocyte migration at 24 h into the lower chamber containing DCs challenged with HAdV5, IgGs or decreasing doses (20×10^3 , 10×10^3 and 5×10^3) of IC-HAdV5 and washed after 30 min post-challenge; data are mean \pm SEM, n = 4 donors; **C)** Representative FCS/SSC profiles of direct DCs (red) pretreated with ZVAD before activation with IC-HAdV5. The CFSE-stained monocytes (blue) were added to the upper compartment and migration was quantified at 24 h; Numbers in dark blue correspond to the percentage of CFSE-labeled monocytes. **D)** Cumulative data from assay in **(C)** n \geq 3 donors; **E)** Representative FCS/SSC profiles of DCs (red) challenged with decreasing doses of IC-HAdV5 or IC-Ad^{L40Q} and CFSE-labeled monocyte (blue) recruitment at 24 h. The numbers in dark blue correspond to the percentage of CFSE-labeled monocytes. **F)** Cumulative data from assay in **(E)** using DCs from \geq 3 donors; **G)** Bystander DCs activated for 12 h with milieu from DC challenged with increasing concentration of IC-HAdV5. The bystander DCs were seeded in the lower chamber of a transwell and CFSE-labeled monocyte recruitment was quantified by flow cytometry at 24 h (n

493 ≥ 4 donors). The numbers in dark blue correspond to the percentage of CFSE-labeled monocytes. **H)**
494 Phenotypic characterization of the monocytes (green cells seeded in the upper chamber) recruited by
495 bystander DCs. DCs were challenged with increasing doses of IC-HAdV5 (colored coded on top of each
496 panel). The milieu from these direct DCs was used to generate bystander DCs. The bystander DCs were
497 seeded in the lower chamber of the transwell system and the monocytes that were recruited were
498 characterized for their expression of CD14 and CD86 at 24 h, and **I)** at 72 h. **J)** Monocytes that did not migrate
499 into the lower chamber were also characterized for the CD14 and CD86 levels. The data are representative
500 flow cytometry profiles of experiments carried out in ≥ 5 donors. p values in **B**, **D**, and **F** were derived from t -
501 tests: * $p < 0.05$, ** $p < 0.01$, and *** $p < 0.001$.

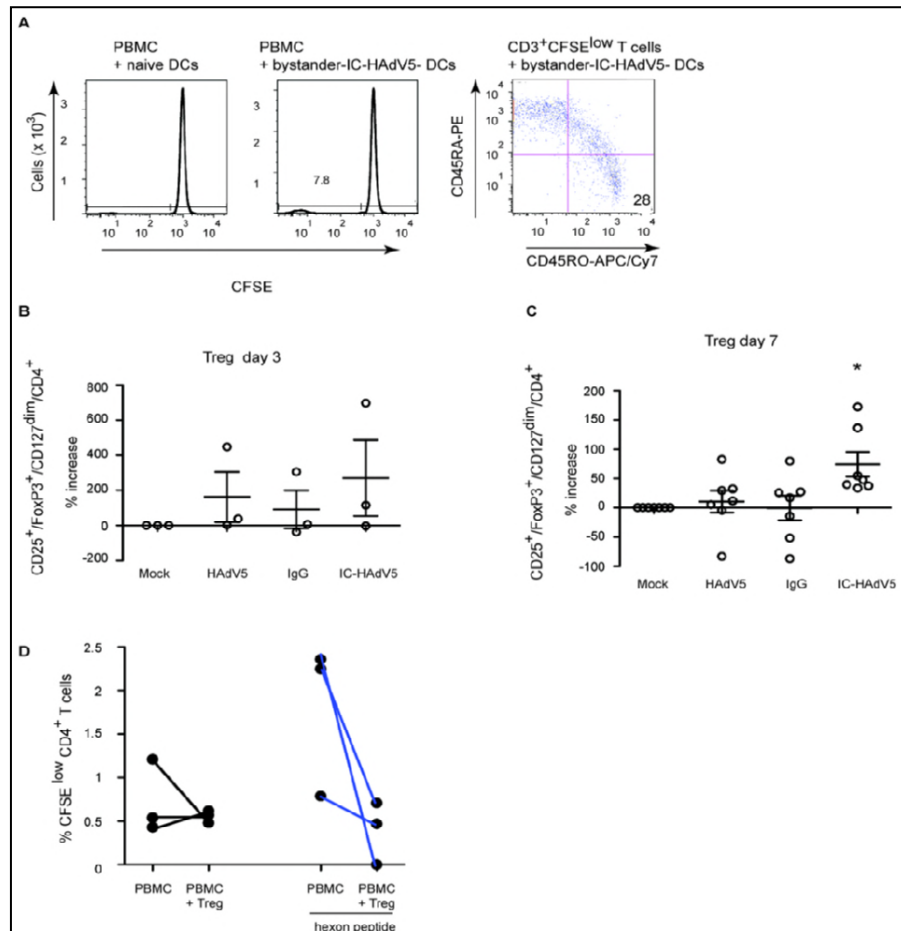
502 **Bystander DCs induce memory T-cell proliferation and naïve CD4 T cells towards** 503 **HAdV-specific T_{regs}**

504 A functional characteristic of tolerogenic DCs is that they take up and present antigens.
505 Therefore, we asked if some of the bystander DCs generated in our ex vivo model are
506 capable of inducing proliferation of HAdV5-specific memory T cells. We used IC-HAdV-
507 challenged DC to generate bystander DCs, which were then added to CFSE-labeled
508 PBMCs. Seven days post-incubation we found that CD3⁺/CFSE^{low} cells harbored memory
509 T cell markers (CD45RO⁺/CD45RA⁻) (**Figure 9A**). These data are consistent with the
510 potential of some of the bystander DCs to maintain fluid phase uptake and subsequent
511 presentation of HAdV5 antigens to memory T cells.

512 In addition to antigen presentation, tolerogenic DCs can induce naïve CD4⁺ cells to
513 become T_{regs}. To address this functional characteristic, bystander DCs were generated
514 and incubated with autologous naïve CD4⁺/CD45RA^{high} cells for 3 or 7 days. The T cells
515 were then assayed by multi-parametric flow cytometry for CD4, CD25, CD127 and FoxP3,
516 markers that are indicative of T_{regs}. While activated T cells transiently express FoxP3
517 (**Figure S9**), the relatively low-level does not result in acquisition of suppressor activity
518 [27]. By contrast, stable and high levels of FoxP3 can be used to identify *bona fide* T_{regs}.
519 At day 3, naïve T cells expressed T_{reg} markers in all conditions (except mock-treated
520 direct DCs) (**Figure 9B**). At day 7, the number cells with T_{reg} phenotype was near
521 background following incubation in the milieu of mock-, IgG-, or HAdV5-challenged direct
522 DC (**Figure 9C**). By contrast, bystander DC created from IC-HAdV-direct DCs had a
523 significant ($p < 0.05$) increase in cells with a T_{reg} profile. This functional assay
524 demonstrates that bystander DCs can induce naïve CD4 into cells with a T_{reg} phenotype,
525 further supporting our conclusion that they are tolerogenic DCs.

526 As shown in **Figure 1D**, healthy adults harbor CD25⁺ cells can inhibit HAdV-specific CD4⁺
527 cell proliferation. We therefore asked if the tolerogenic bystander DCs generated in our ex
528 vivo assay could induce the production of HAdV-specific T_{regs}. To address this question
529 we isolated PBMCs, CD14⁺ monocytes, and naïve CD4⁺ T cells from 3 donors that
530 harbored anti-HAdV memory T cells (see **Figure S10** for flow chart). Briefly, monocytes
531 were used to create direct DCs that were incubated with IC-HAdV-C5. Bystander DCs

532 were generated as previously described. VPD 450-labeled naïve CD4⁺ T cells were
 533 incubated with bystander DCs to generate T_{regs}. VPD 450^{low}/CD4⁺/CD25⁺ cells (600 to
 534 5,000 cells) were isolated by FACS and mixed with CFSE-labeled PBMCs ± hexon
 535 peptides. We found that the ex vivo generated T_{regs} from all donors reduced the
 536 proliferation of anti-HAdV T cells (CFSE^{low}/CD4⁺) (**Figure 9D**). These data demonstrate
 537 that HAdV-specific T_{regs} can be generated via bystander DCs.



538

539 **Figure 9) Bystander DCs induce memory T cell proliferation and promote naïve CD4 cells towards T_{reg}**
 540 **phenotype that inhibit proliferation of anti-HAdV T cells**

541 **A)** Bystander DCs, generated via IC-HAdV stimulation of direct DCs or mock-treated DCs, were incubated
 542 with CFSE-labeled PBMCs and proliferation was quantified by flow cytometry. CD3⁺/CFSE^{low} cells were
 543 screened for memory T cell profile (CD45RO vs. CD45RA). Bystander DCs, generated using the media from
 544 DCs challenged with IgG, HAdV5, and IC-HAdV5, were incubated with 10⁵ naïve CD4⁺ T (ratio of 10:1 PBMC/
 545 bystander DC) cells isolated from the same donors.

547 The percentage of T_{regs} (CD25⁺/FoxP3^{high}/CD127^{dim}/CD4⁺ cells) varies between 1 to 5% of CD4⁺ cells in
 548 peripheral blood. The number of T_{regs} in the CD4⁺ cell population, ± bystander DCs, was quantified by
 549 analyzing 50,000 cells by flow cytometry. The results are presented as percentage of increase of mock-
 550 treated cells at day 3 (**B**) or day 7 (**C**).

551 **D)** T_{regs} generated by bystander DCs reduce the proliferation of memory anti-HAdV CD4⁺ T cells.

552 Experiments were carried out in ≥7 donors with similar results. * *p* < 0.05 vs. mock, HAdV5 and IgG.

553 Discussion

554 HAdV infections lead to multifaceted, robust, long-lived cellular and humoral responses in
555 most young immunocompetent adults. Nonetheless, several HAdV types somehow
556 circumvent immune surveillance to establish persistent infections. It is well documented
557 that HAdV neutralizing antibodies are type specific, while the anti-HAdV cellular response
558 is cross-reactive [1,3,8,47–49]. In addition, it is the anti-HAdV cellular response that
559 protects us from reactivation of persistent infections. The dichotomy between the two
560 arms of the adaptive immune response led us to address how anti-HAdV antibodies
561 influence HAdV-specific T-cell responses. In this study, we initially asked if healthy adults
562 harbor HAdV-specific T_{regs} , which would be indicative of a path towards HAdV
563 persistence. We then explored how HAdV-specific tolerogenic DCs and T_{regs} could be
564 generated. We previously showed that IC-HAdV5s are internalized by, and aggregate in,
565 DCs [14]. Following protein VI-dependent endosomal escape of the capsid, the viral
566 genome is engaged by AIM2 in the cytoplasm. AIM2 nucleation induces ASC (apoptosis-
567 associated speck protein containing a caspase activation/recruitment domain)
568 aggregation, inflammasome formation, caspase 1 auto-activation, pro-IL-1 β and GSDMD
569 cleavage, and GSDMD-mediated loss of cell membrane integrity. Here we demonstrate
570 that the pyroptotic environment plays a significant role the creation of tolerogenic
571 bystander DCs. We further show that these bystander DCs can induce HAdV5-specific
572 memory T cells to proliferate, and can drive naïve CD4 cells towards a T_{reg} phenotype.
573 The T_{regs} generated in this *ex vivo* assay are capable of inhibiting the proliferation of anti-
574 HAdV T cells. We therefore propose that HAdV neutralizing IgGs [14] abet HAdV
575 persistence.

576 Our assays using a human pathogen, naturally occurring human antibodies and primary
577 blood-derived human cells address the immune cell-based mechanisms of adenovirus
578 persistence. Yet, *ex vivo* results cannot unequivocally show causality. Host-pathogen-
579 based studies have often used mice to address questions underlying disease-immune
580 relationships. However, the impact of HAdVs on human and mouse DCs is notably
581 different. Furthermore, we are unaware of studies directing addressing the impact of
582 murine adenovirus (MAV) on murine DCs. In 1964, D. Ginder showed that a MAV can
583 cause persistent infections for 10 weeks in outbred Swiss mice [50]. K. Spindler and
584 colleagues then showed that MAV-1 infections persist for at least 55 weeks in outbred
585 Swiss mice [51]. In addition, Spindler and colleagues demonstrated that in contrast to
586 humans, mice that lack B cells are highly susceptible to MAV-1 infection, while mice that
587 lack T cells are not susceptible [52]. In light of our results, the question could be raised as
588 to whether anti-MAV-1 antibodies are needed to generate T_{regs} to reduce the potential

589 impact T-cell induced immunopathology [27]. To address this one could use a single pre-
590 injection of sera from MAV-1-challenged mice into B-cell deficient mice and quantify
591 disease progression. Using nonhuman primates (NHPs) to address the dichotomy
592 between the two arms of the adaptive immune response to adenoviruses is likely a more
593 informative option, but use of NHPs entails unique challenges when it comes to pre-
594 existing exposure to their own set of adenoviruses. Nonetheless, Miller and colleagues
595 elegantly showed that NHPs, harboring neutralizing antibody response against a HAdV5
596 host-range mutant, and then re-challenged with the same virus, respond with a significant
597 increase in circulating T_{regs} [53]. These *in vivo* observations, which hinge on the pre-
598 existing neutralizing antibodies, are consistent with our proposed mechanism. One also
599 needs to take into the dynamic, recurrent exposure to HAdVs during childhood and
600 adolescence. These encounters provide multiple opportunities for the formation of IC-
601 HAdVs and the impetus to form HAdV-specific tolerogenic DCs and T_{regs}.

602 Our data also complement the mechanism for HAdV5 persistence described by Hearing
603 and colleagues [6]. Using human cell lines, they showed that IFN- α and IFN- γ production
604 block HAdV5 replication via an E2F/Rb transcriptional repression of its E1A immediate
605 early gene [54]. The E1A gene product is essential for activating expression of the other
606 early genes and reprogramming the cell into a state that allows virus propagation. Of note,
607 type 1 IFN secretion is significant from IC-HAdV5-challenged DCs and may allow HAdVs
608 (including those that are covered with non-neutralizing Abs) to be taken up by neighboring
609 cells to establish persistent infections.

610 Mechanisms by which DCs promote tolerance include induction of T_{regs}, the inhibition of
611 memory T-cell responses, T-cell anergy, and clonal deletion [24–26]. The semi-mature
612 phenotype of tolerogenic DCs provide insufficient stimulatory signals and drive naïve T
613 cells to differentiate into T_{regs} rather than effector T cells [55]. The global anti-viral
614 response by DCs acts via a combinatorial cytokine code to direct the response of
615 neighboring immune cells. The cytokine profile produced by the IC-HAdV5-challenged
616 DCs and bystander DCs is noteworthy, particularly in the context of the combination and
617 dose that influences activation of other immune cells. Recently, a biochemical and
618 functional chemokine interactome study suggested that several chemokines form
619 heterodimers that have unique functions in certain conditions [56]. Based on these
620 interactome data, we plotted the possible combinations that could influence the direct and
621 bystander DCs in our assays (**Figure S11**). What impact these heterodimers could have
622 on HAdV persistence will require future study, in particular because we did not find
623 notable levels of TGF β secreted by direct or bystander DCs. More than other cytokine
624 families, the IL-1 family may be primordial because it is tightly linked to IC-HAdV-induced

625 DC pyroptosis. Indeed, the intracellular domain of the IL-1R1 shares similar signaling
626 function properties with TLRs. In general, IL-1 β release from monocytes is tightly
627 controlled; less than 20% of the total pro-IL-1 β precursor is processed and released. IL-1 β
628 also increases the expression of intercellular adhesion molecule-1 and vascular cell
629 adhesion molecule-1, which, together with the chemokines, promote the infiltration of
630 cells from the circulation into the extravascular space and then into inflamed tissues [57].
631 While circulating monocytes do not constitutively express *IL1 β* mRNA, adhesion to
632 surfaces during diapedesis induces the synthesis of large amounts that are assembled
633 into large polyribosomes primed for translation [58].

634 Two aspects of the IC-HAdV-induced DC immune response that remain unknown are the
635 impact of neutrophils and the phenotype/function of recruited monocytes. Neutrophils are
636 pertinent because they can secrete/release proteinase 3 (PR3), elastase, cathepsin-G,
637 chymase, chymotrypsin, and meprin α or β , which can process extracellular pro-IL-1 β into
638 its active form [59,60]. In addition, IC-HAdVs activate neutrophils (L-selectin shedding) via
639 Fc receptors and complement receptor 1 interactions [61]. Moreover, neutrophils are a
640 major source for anti-microbial peptides (e.g., defensins and LL-37) and proteins (e.g.
641 lactoferrin) for which a pro- or anti-viral roles in HAdV infection has been proposed [62].
642 With respect to the phenotype/function of recruited monocytes, Ly6C^{hi} monocytes [63],
643 which suppress T-cell proliferation during HAdV-induced inflammation [64], may also
644 impact the creation of HAdV antigen-presenting tolerogenic DCs and HAdV-specific T_{regs}.

645 The dynamic equilibrium between recurrent HAdV infections and IC-HAdV formation, DC
646 maturation/pyroptosis, recruitment and generation of bystander DC, and T_{regs}
647 production/activation, likely starts in childhood and develops nonlinearly over decades.
648 While it is hard to argue that the generation of persistent infections is not beneficial to the
649 pathogen, it is possible that the sustained anti-HAdV cellular and humoral responses
650 partially shield a healthy host from infections by other pathogens (e.g. hepatitis C virus
651 [65]) or the related immune-induced tissue damage [66]. Avoiding chronic tissue damage
652 is particularly important because, as mentioned previously, HAdVs infect the eye,
653 respiratory and gastrointestinal tracts. However, in a T-cell compromised host IC-HAdV-
654 induced pyroptosis of Fc γ R⁺ cells (neutrophils, monocytes, macrophages, DCs) may also
655 prime the host for HAdV-disseminated disease.

656 In summary, our findings suggest a mechanism by which humoral immunity to HAdV
657 fosters tolerance. Understanding this complex virus-host interplay may enable us to
658 identify high risk patients undergoing immunosuppression and develop therapies to treat
659 disseminated HAdV-disease [67,68].

660 **Materials and Methods**

661 **Ethics statement**

662 Blood samples from >120 anonymous donors from the local blood bank (Etablissement
663 Français du sang, Montpellier, France) were used during this study. All donors provided
664 written informed consent.

665 **Cells and culture conditions**

666 DCs were generated from freshly isolated CD14⁺ monocytes in the presence of 50 ng/ml
667 granulocyte-macrophage colony-stimulating factor (GM-CSF) and 20 ng/ml interleukin-4
668 (IL-4) (PeproTech, Neuilly sur Seine, France) [3]. DC stimulations were performed 6 days
669 post-isolation of monocytes. THP-1 cells purchased from ATCC (TIB-202) were cultured in
670 RPMI 1640 medium supplemented with 10% fetal bovine serum (FBS). Similar to DCs,
671 THP-1 cells were differentiated into DCs using 50 ng/ml GM-CSF and 20 ng/ml IL-4 for 6
672 days.

673 **HAdV vectors & hexon peptides**

674 Ad β gal is a Δ E1/E3 HAdV5 vector harboring a *lacZ* expression cassette [69]. Ad^{L40Q} is an
675 HAdV5-based vector with a leucine to glutamine mutation of an amino acid in protein VI
676 that decreases its membrane lytic activity [31]. Alexa555- and Alexa488-HAdV5 were
677 generated from Ad β gal by using an Alexa555 or Alexa488 Protein Labeling Kit (Life
678 Technologies, Villebon-sur-Yvette, France) as previously described [70]. Ad2ts1 harbors a
679 mutation in protease and results in several unprocessed capsid proteins and a hyper-
680 stable capsid [71]. All HAdV viruses/vectors were produced in 293 or 911 cells and
681 purified by double banding on CsCl density gradients as previously describe [14]. Vector
682 purity typically reaches >99%. HAdV concentrations (physical particles/ml) were
683 determined as previously described [72]. The hexon peptide pool (PepTivator AdV5
684 hexon, Miltenyi) is overlapping sequences of the HAdV5 hexon protein.

685 **Antibodies**

686 Anti-human CD4-PE, anti-human CD83-FITC (cat 556910), anti-human HLA-ABC-PE (cat
687 555553), anti-human HLA-DR-PE (cat 555812), anti-human CD80-FITC (cat 557226),
688 anti-human CD86-APC (cat 555660), anti-human CD25-PE (cat 555432), anti-human
689 CD127-FITC (cat 561697), anti-human CD4-PE-Cy7 (BD) (cat 348809), anti-TNF-PE-Cy7
690 (cat 557647), anti-IL-2-PE (cat 554566), anti-IFN- γ -APC (cat 554702), anti-IL-10-PE (cat
691 554706) were from Becton Dickinson, Pharmigen. Anti-human Foxp3-APC (cat 17-4776-
692 41) was from eBioscience. Anti-human CD14-PE (cat A07764) was from Beckman
693 Coulter. Anti-human CD45RO-APC/Cy7 (cat 304227), anti-human CD45RA-PE (cat

694 304205), anti-human CD3-APC (cat 300411), and anti-human CD40-APC (cat 313008)
695 were from BioLegend).

696 **Immune complex formation and DC stimulations**

697 DCs (4×10^5 in 400 μ l of complete medium) were incubated with HAdV5 or IC-HAdV5 (or
698 IC) (2×10^4 physical particles (pp)/cell, unless otherwise indicated) for the indicated times.
699 IC-HAdV5s were generated by mixing the virus (8×10^9 physical particles) with 2.5 μ l of
700 IVIg (human IgG pooled from 1,000 to 50,000 donors/batch) (Baxter SAS, Guyancourt,
701 France) for 15 min at room temperature. IVIg is used in patients with primary or acquired
702 immunodeficiency as well as autoimmune diseases. Z-VAD-FMK 20 μ M (ZVAD) was
703 added 2 h before stimulation. Brefeldin A was used at 3 μ g/ml after 6 h stimulation or for
704 the same time with stimulation.

705 **Bystander DC stimulation**

706 DCs (1.5×10^6 in 1.5 ml of full media) were incubated \pm LPS 100 ng/ml, HAdV5, and IgG
707 in the lower compartment of the well (12 mm diameter polyester membranes with 0.4 μ m
708 pores; (Corning, Bagnaux-sur-Loing, France). After 6 h incubation, fresh immature DCs
709 (6×10^5 in 600 μ l of media) were added to the upper compartment and are referred to as
710 bystander DCs. TAK-242 was added to DCs 1 h pre-challenge.

711 **Quantification of mRNA**

712 Expression levels of cytokine and chemokine genes were evaluated using RT-qPCR
713 assays. Total RNA was isolated from cells using the high pure RNA isolation Kit (Roche,
714 Berlin, Germany) with a DNase I treatment during the purification and subsequent elution
715 in 50 μ l of RNase-free water (Qiagen, IN, USA). Reverse transcription was performed with
716 the superscript first-strand synthesis system (Invitrogen) using 10 μ l of total RNA and
717 random hexamers. The cDNA samples were diluted 1:20 in water and analyzed in
718 triplicate using a LightCycler 480 (Roche, Meylan, France). SYBR green PCR conditions
719 were as follows: 95°C for 5 min and 45 cycles of 95°C for 15 s, 65°C or 70°C for 15 s, and
720 72°C for 15 s using *GAPDH* as a standard. See **Table S2** for primers sequencers.
721 Relative gene expression levels of each respective gene were calculated using the
722 threshold cycle ($2^{-\Delta\Delta CT}$) method and normalized to *GAPDH* mRNA levels.

723 **RT² Profiler™ PCR array**

724 Expression levels of cytokine and chemokine mRNAs were analyzed using PCR array
725 assays. Total RNA was isolated from cells using the High Pure RNA isolation Kit (Roche,
726 Berlin, Germany) with a DNase I treatment during the purification and elution in 50 μ l of
727 RNase-free water (Qiagen). Reverse transcription was performed with the RT² First strand

728 Kit (Qiagen, Courtaboeuf, France), and the cDNA samples were analyzed in duplicate
729 using a RT² Profiler™ PCR array (Qiagen). SYBR green PCR conditions were 95°C for
730 10 min and 40 cycles of 95°C for 15 s, and 60°C for 1 min using 84 human inflammatory
731 and receptor genes. The potential mRNAs were chosen and then confirmed by RT-qPCR.

732 The genes that contributed in each axis in the PCA were as follows: **F1** = *CCL1, 2, 4, 5, 7*
733 *13, 15, 17, 20, 22, CSF1, CX3CL1, CXCL 1 to 3, 5, 8 to 11, FASLG, IFNG, IL10RA,*
734 *IL10RB, IL15, IL1a, IL1b, IL7, NAMPT, TNFSF4, 10, 11, 13, 13B, and VEGFA. F2 =
735 *AIMP1, C5, CCL1, 2, 13, 17, 23, CRR1, 2, 3, 4, 5, CSF1, CX3CR1, CXCR2, IL10RA,*
736 *I10RB, IL15, LTA, LTB, MIF, SPP1, TNF, TNFSF4, 10, 11, 13, and 13B. F3 = *CCL17, 23,*
737 *CCR5, CX3CR1, IL10RA, IL5, IL9, MIF, and OSM.***

738 **Co-stimulatory protein levels**

739 Surface levels of CD83, MHCII, CD80, CD40, and CD86 were assessed by flow
740 cytometry. Cell membrane integrity was assessed by collecting cells via centrifugation at
741 800x g; the cell pellets were then resuspended in PBS containing 10% FBS, propidium
742 iodide (PI) (Sigma-Aldrich, Missouri, USA), or 7-aminoactinomycin D (7AAD) (Becton-
743 Dickinson, New Jersey, USA). The cell suspension was incubated for the indicated times
744 and analyzed using a FacsCalibur flow cytometer (Becton-Dickinson) and FlowJo
745 software.

746 **Intracellular staining**

747 Surface and intracellular levels of CD83 and CD86 (total protein) were stained with a BD
748 Cytotfix/Cytoperm™ Fixation/Permeabilization Kit, and then measured by flow cytometry.
749 To assess cell membrane integrity, the cells were collected and centrifuged at a speed of
750 800x g; the cell pellets were then resuspended in PBS, 10% FBS, PI (Sigma), or 7AAD
751 and analyzed on a FacsCalibur flow cytometer (Becton-Dickinson) and FlowJo software.

752 **Monocyte migration assay**

753 Monocyte migration was evaluated using a 5.0 µm-diameter pore transwell system
754 (Corning, Bagnaux-sur-Loing, France). Monocytes (2×10^5 in 200 µl of full media) were
755 added into inserts and DCs or DCs (7.5×10^5 in 750 µl of full media) and \pm LPS (100
756 ng/ml), HAdV5, HAd555, or IgG in the lower wells. Monocytes were stained by carboxy-
757 fluorescein diacetate-succinimidyl ester (CFSE) (Molecular Probes, Eugene, OR, USA)
758 (CellTrace™ CFSE Cell Proliferation Kit). DCs incubated for 30 min with HAd555 or
759 HAdV5 and IgG in the lower chamber were or were not washed in medium before adding
760 the stained CFSE monocytes. After 3, 6, and 24 h incubation at 37°C, the cells in the

761 upper and lower compartment were detected quantified using a FacsCalibur flow
762 cytometer (Becton-Dickinson) and FlowJo software.

763 **Cytokine secretion: ELISA and Luminex assays**

764 Supernatant from the cells were collected and cytokine secretion was measured by ELISA
765 and Luminex assays. The secretion of TNF and IL-1 β was quantified by ELISA using an
766 OptEIA human TNF ELISA Kit (Becton Dickinson) and human IL-1 β /IL-1F2 DuoSet ELISA
767 (R&D Systems, Lille, France) following the manufacturer's instructions. Additionally, 22
768 other cytokines and chemokines were detected by Luminex using a Bio-plex pro human
769 chemokine, cytokine kit (Bio-Rad, Marnes-La-Coquette, France) following the
770 manufacturer' instructions.

771 **Depletion of CD25⁺ from PBMC**

772 PBMC were isolated using standard gradient separation techniques. Half were CD25⁺-
773 depleted, using anti-CD25 in a human CD4⁺CD25⁺CD127^{dim/-} Regulatory T Cell Isolation
774 Kit II and MACS separation system.

775 **CFSE and VPD 450 labeling**

776 PBMCs were washed and suspended in PBS for labeling with CFSE or Violet Proliferation
777 Dye 450 (VPD 450) (BD Horizon™, Le Pont de Claix, France) at a final concentration of
778 2.5 μ M or 1 μ M, respectively, for 3 min at room temperature. Labeling was terminated by
779 the addition of fetal calf serum (FCS) (40% of total volume).

780 **PBMC activation assays**

781 PBMCs \pm CD25⁺ were stained with CFSE and cultivated in 96-well U-bottom plates; (cell
782 concentration 1 x 10⁶/ml and a final volume of 200 μ l; PBMC CD25⁺/ PBMC CD25⁻ ratio
783 1:10). HAdV5 hexon peptides (PepTivator, Miltenyi, Paris, France) were added at 0.3
784 nmol. On days 3 and 5 the cells were split and IL-2 was added (final concentration 100
785 U/ml). Cells were analyzed on a FACS Canto II using FlowJo software.

786 **T_{reg} generation**

787 Naïve CD4⁺ T cell were isolated using naïve CD4⁺ T Cell Isolation Kit II and MACS
788 separation system. DCs indirectly activated for 12 h with LPS, HAdV5, IC-HAdV5 and IgG,
789 and then were co-cultured with CD4⁺ naïve T cells labeled VPD450 (with ratio bystander
790 DCs/ T cells is 3:1) in RPMI 1640 supplemented with 10% FCS and IL-2 (Proleukin 18 x
791 10⁶ IU, CA, USA) (100 U/ml) for 3 or 7 days. Recombinant IL-2 was added on day 3 and
792 day 5. CD25, CD127, and FoxP3 levels were quantified by flow cytometry using FACS
793 Canto II.

794 **Statistical analyses**

795 All experiments were performed at least in duplicate a minimum of three independent
796 times, and the results are expressed as mean \pm SEM unless otherwise stated. The
797 statistical analyses were performed using the Student's *t*-test unless otherwise stated. A *p*
798 value < 0.05 is denoted as significant. Statistical analyses of the global cytokine profiles
799 (pie chart) were performed by partial permutation tests using the SPICE software.

800 **Data availability**

801 All data generated or analyzed during this study are included in this published article (and
802 its supplementary information files).

803 **Acknowledgments**

804 We thank Sylvie Grandemange, Fabien Blanchet, Sebastian Nisole, Valerie Dardalhon,
805 and Claire Daien for reagents and advice. We thank EKL members for technical help and
806 constructive comments. We thank the MRI, member of the national infrastructure France-
807 Biolmaging, and SERENAD for statistical analyses. KE current address: Vaccine and
808 Infectious Disease Division, Fred Hutchinson Cancer Research Center, Seattle, WA, USA.

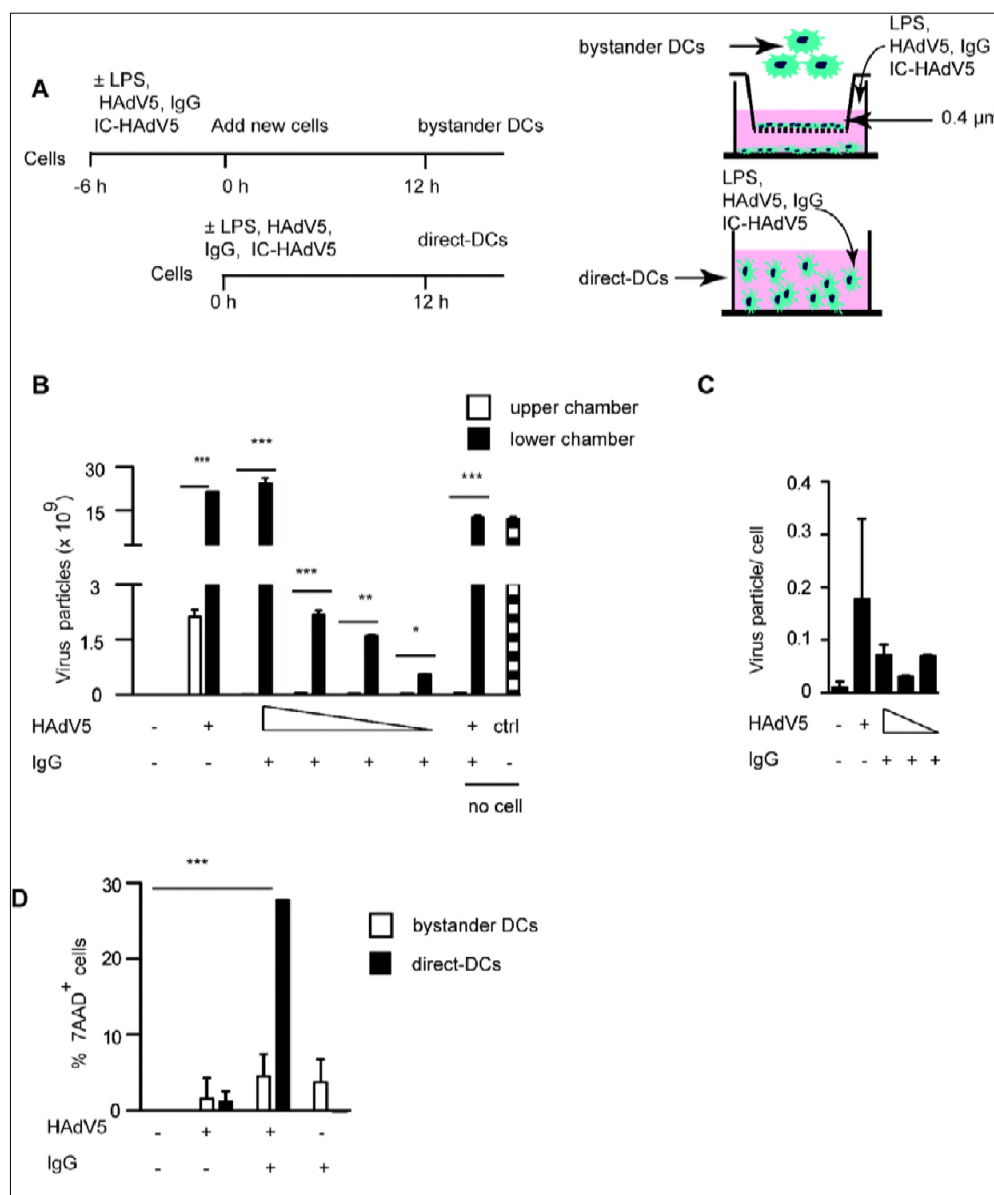
809 References

- 810 1. Flomenberg P, Piaskowski V, Truitt RL, Casper JT. Characterization of human proliferative T cell responses to
811 adenovirus. *J Infect Dis.* 1995;171: 1090–1096.
- 812 2. Tang J, Olive M, Pulmanusahakul R, Schnell M, Flomenberg N, Eisenlohr L, et al. Human CD8+ cytotoxic T cell
813 responses to adenovirus capsid proteins. *Virology.* 2006;350: 312–322. doi:10.1016/j.virol.2006.01.024
- 814 3. Perreau M, Kremer EJ. Frequency, Proliferation, and Activation of Human Memory T Cells Induced by a
815 Nonhuman Adenovirus. *J Virol.* 2005;79: 14595–14605. doi:10.1128/JVI.79.23.14595-14605.2005
- 816 4. Lion T. Adenovirus infections in immunocompetent and immunocompromised patients. *Clin Microbiol Rev.*
817 2014;27: 441–462. doi:10.1128/CMR.00116-13
- 818 5. King CR, Zhang A, Mymryk JS. The persistent mystery of adenovirus persistence. *Trends Microbiol.* 2016;24: 323–
819 324. doi:10.1016/j.tim.2016.02.007
- 820 6. Zheng Y, Stamminger T, Hearing P. E2F/Rb Family Proteins Mediate Interferon Induced Repression of Adenovirus
821 Immediate Early Transcription to Promote Persistent Viral Infection. *PLoS Pathog.* 2016;12: 1–24.
822 doi:10.1371/journal.ppat.1005415
- 823 7. Veltrop-Duits LA, Van Vreeswijk T, Heemskerk B, Thijssen JCP, Seady R El, Jol-Van Der Zijde EM, et al. High
824 titers of pre-existing adenovirus serotype-specific neutralizing antibodies in the host predict viral reactivation after
825 allogeneic stem cell transplantation in children. *Clin Infect Dis.* 2011;52: 1405–1413. doi:10.1093/cid/cir231
- 826 8. Leen AM, Sili U, Vanin EF, Jewell AM, Xie W, Vignali D, et al. Conserved CTL epitopes on the adenovirus hexon
827 protein expand subgroup cross-reactive and subgroup-specific CD8+ T cells. *Blood.* 2004;104: 2432–2440.
828 doi:10.1182/blood-2004-02-0646
- 829 9. Leen AM, Myers GD, Sili U, Huls MH, Weiss H, Leung KS, et al. Monoculture-derived T lymphocytes specific for
830 multiple viruses expand and produce clinically relevant effects in immunocompromised individuals. *Nat Med.*
831 2006/09/26. 2006;12: 1160–1166. doi:10.1038/nm1475
- 832 10. Cichon G, Boeckh-Herwig S, Schmidt HH, Wehnes E, Muller T, Pring-Akerblom P, et al. Complement activation by
833 recombinant adenoviruses. *Gene Ther.* 2001;8: 1794–1800.
- 834 11. Mistchenko AS, Lenzi HL, Thompson FM, Mota EM, Vidaurreta S, Navari C, et al. Participation of immune
835 complexes in adenovirus infection. *Acta Paediatr.* 1992;81: 983–988. doi:10.1111/j.1651-2227.1992.tb12159.x
- 836 12. Mistchenko AS, Diez RA, Mariani AL, Robaldo J, Maffey AF, Bayley-Bustamante G, et al. Cytokines in adenoviral
837 disease in children: association of interleukin-6, interleukin-8, and tumor necrosis factor alpha levels with clinical
838 outcome. *J Pediatr.* 1994;124: 714–720. doi:S0022347694000120
- 839 13. Perreau M, Pantaleo G, Kremer EJ. Activation of a dendritic cell–T cell axis by Ad5 immune complexes creates an
840 improved environment for replication of HIV in T cells. *J Exp Med.* 2008;205: 2717–2725.
841 doi:10.1084/jem.20081786
- 842 14. Eichholz K, Bru T, Tran TTP, Fernandes P, Welles H, Mennechet FJD, et al. Immune-complexed adenovirus
843 induce AIM2-mediated pyroptosis in human dendritic cells. *PLoS Pathog.* 2016;12: e1005871.
844 doi:10.1371/journal.ppat.1005871
- 845 15. Schuurhuis DH, van Montfoort N, Ioan-Facsinay A, Jiawan R, Camps M, Nouta J, et al. Immune complex-loaded
846 dendritic cells are superior to soluble immune complexes as antitumor vaccine. *J Immunol.* 2006;176: 4573–4580.
- 847 16. Fernandes-Alnemri T, Yu J-W, Datta P, Wu J, Alnemri ES. AIM2 activates the inflammasome and cell death in
848 response to cytoplasmic DNA. *Nature.* 2009;458: 509–513. doi:10.1038/nature07710
- 849 17. Bergsbaken T, Fink SL, Cookson BT. Pyroptosis: host cell death and inflammation. *Nat Rev Microbiol.* 2009;7: 99–
850 109. doi:10.1038/nrmicro2070
- 851 18. Unterholzner L. The interferon response to intracellular DNA: Why so many receptors? *Immunobiology.* 2013;218:
852 1312–1321. doi:10.1016/j.imbio.2013.07.007
- 853 19. Shi J, Zhao Y, Wang K, Shi X, Wang Y, Huang H, et al. Cleavage of GSDMD by inflammatory caspases
854 determines pyroptotic cell death. *Nature.* 2015;526: 660–665. doi:10.1038/nature15514
- 855 20. Belkaid Y. Regulatory T cells and infection: a dangerous necessity. *Nat Rev Immunol.* 2007;7: 875–888.
856 doi:10.1038/nri2189
- 857 21. Raker VK, Domogalla MP, Steinbrink K. Tolerogenic dendritic cells for regulatory T cell induction in man. *Front*
858 *Immunol.* 2015;6: 1–11. doi:10.3389/fimmu.2015.00569
- 859 22. Li S, Gowans EJ, Chougnet C, Plebanski M, Dittmer U. Natural regulatory T cells and persistent viral infection. *J*
860 *Viro.* 2008;82: 21–30. doi:10.1128/JVI.01768-07
- 861 23. Yadav M, Stephan S, Bluestone JA. Peripherally induced Tregs-role in immune homeostasis and autoimmunity.
862 *Front Immunol.* 2013;4: 1–12. doi:10.3389/fimmu.2013.00232
- 863 24. Lutz MB, Schuler G. Immature, semi-mature and fully mature dendritic cells: Which signals induce tolerance or
864 immunity? *Trends in Immunology.* 2002. pp. 445–449. doi:10.1016/S1471-4906(02)02281-0
- 865 25. Ma Y, Shurin G V., Gutkin DW, Shurin MR. Tumor associated regulatory dendritic cells. *Seminars in Cancer*
866 *Biology.* 2012. pp. 298–306. doi:10.1016/j.semcancer.2012.02.010
- 867 26. Kanamori M, Nakatsukasa H, Okada M, Lu Q, Yoshimura A. Induced Regulatory T Cells: Their Development,
868 Stability, and Applications. *Trends Immunol.* 2016;37: 803–811. doi:10.1016/j.it.2016.08.012
- 869 27. Josefowicz SZ, Lu LF, Rudensky AY. Regulatory T cells: mechanisms of differentiation and function. *Annu Rev*
870 *Immunol.* 2012;30: 531–564. doi:10.1146/annurev.immunol.25.022106.141623
- 871 28. Iberg CA, Jones A, Hawiger D. Dendritic Cells As Inducers of Peripheral Tolerance. *Trends in Immunology.* 18 Aug
872 2017: 1–12. doi:10.1016/j.it.2017.07.007
- 873 29. Perreau M, Mennechet F, Serratrice N, Glasgow JN, Curiel DT, Wodrich H, et al. Contrasting Effects of Human,

- 874 Canine, and Hybrid Adenovirus Vectors on the Phenotypical and Functional Maturation of Human Dendritic Cells:
875 Implications for Clinical Efficacy. *J Virol.* 2007;81: 3272–3284. doi:10.1128/JVI.01530-06
- 876 30. Domogalla MP, Rostan P V., Raker VK, Steinbrink K. Tolerance through education: How tolerogenic dendritic cells
877 shape immunity. *Frontiers in Immunology.* 2017. doi:10.3389/fimmu.2017.01764
- 878 31. Moyer CL, Wiethoff CM, Maier O, Smith JG, Nemerow GR. Functional genetic and biophysical analyses of
879 membrane disruption by human adenovirus. *J Virol.* 2011;85: 2631–2641. doi:10.1128/JVI.02321-10
- 880 32. Mangel WF, San Martin C. Structure, function and dynamics in adenovirus maturation. *Viruses.* 2014;6: 4536–
881 4570. doi:10.3390/v6114536
- 882 33. Ortega-Esteban A, Bodensiek K, San Martín C, Suomalainen M, Greber UF, de Pablo PJ, et al. Fluorescence
883 tracking of genome release during the mechanical unpacking of single viruses. *ACS Nano.* 2015;24: 10571–9.
884 doi:10.1021/acs.nano.5b03020
- 885 34. Ohashi K, Burkart V, Flohe S, Kolb H. Cutting Edge: Heat Shock Protein 60 Is a Putative Endogenous Ligand of
886 the Toll-Like Receptor-4 Complex. *J Immunol.* 2000;164: 558–561. doi:10.4049/jimmunol.164.2.558
- 887 35. Roelofs MF, Boelens WC, Joosten L, Abdollahi-Roodsaz S, Geurts J, Wunderink LU, et al. Identification of Small
888 Heat Shock Protein B8 (HSP22) as a Novel TLR4 Ligand and Potential Involvement in the Pathogenesis of
889 Rheumatoid Arthritis. *J Immunol.* 2006;176: 7021–7027. doi:10.4049/jimmunol.176.11.7021
- 890 36. Park JS, Gamboni-Robertson F, He Q, Svetkauskaite D, Kim J-Y, Strassheim D, et al. High mobility group box 1
891 protein interacts with multiple Toll-like receptors. *Am J Physiol Cell Physiol.* 2006;290: C917–C924.
892 doi:10.1152/ajpcell.00401.2005
- 893 37. Rallabhandi P, Phillips RL, Marina S. Respiratory Syncytial Virus Fusion Protein-Induced Toll-Like Receptor 4
894 (TLR4) Signaling Is Inhibited by the TLR4 Antagonists *Rhodobacter sphaeroides* Lipopolysaccharide and Eritoran
895 (E5564) and Requires Direct Interaction with MD-2. *MBio.* 2012;3: e00218–12. doi:10.1128/mBio.00218-12.Editor
- 896 38. Shimazu R, Akashi S, Ogata H, Nagai Y, Fukudome K, Miyake K, et al. MD-2, a Molecule that Confers
897 Lipopolysaccharide Responsiveness on Toll-like Receptor 4. *J Exp Med.* 1999;189: 1777–1782.
898 doi:10.1084/jem.189.11.1777
- 899 39. Deguchi A, Tomita T, Omori T, Komatsu A, Ohto U, Takahashi S, et al. Serum amyloid A3 binds MD-2 to activate
900 p38 and NF- κ B pathways in a MyD88-dependent manner. *J Immunol.* 2013;191: 1856–1864.
901 doi:10.4049/jimmunol.1201996
- 902 40. Hiratsuka S, Watanabe A, Sakurai Y, Akashi-Takamura S, Ishibashi S, Miyake K, et al. The S100A8-serum
903 amyloid A3-TLR4 paracrine cascade establishes a pre-metastatic phase. *Nat Cell Biol.* 2008;10: 1349–1355.
904 doi:10.1038/ncb1794
- 905 41. Eichholz K, Mennechet FJD, Kremer EJ. Human Coagulation Factor X-Adenovirus Type 5 Complexes Poorly
906 Stimulate an Innate Immune Response in Human Mononuclear Phagocytes. *J Virol.* 2015;89: 2884–2891.
907 doi:10.1128/JVI.03576-14
- 908 42. Sallusto F, Cella M, Danieli C, Lanzavecchia A. Dendritic cells use macropinocytosis and the mannose receptor to
909 concentrate macromolecules in the major histocompatibility complex class II compartment: downregulation by
910 cytokines and bacterial products. *J Exp Med.* 1995;182: 389–400. doi:10.1084/jem.182.2.389
- 911 43. Min WP, Zhou D, Ichim TE, Strejan GH, Xia X, Yang J, et al. Inhibitory feedback loop between tolerogenic dendritic
912 cells and regulatory T cells in transplant tolerance. *J Immunol.* 2003;170: 1304–1312.
913 doi:10.4049/jimmunol.170.3.1304
- 914 44. Shi C, Pamer EG. Monocyte recruitment during infection and inflammation. *Nat Rev Immunol.* 2011;11: 762–774.
915 doi:10.1038/nri3070
- 916 45. Danella Polli C, Alves Toledo K, Franco LH, Sammartino Mariano V, de Oliveira LL, Soares Bernardes E, et al.
917 Monocyte Migration Driven by Galectin-3 Occurs through Distinct Mechanisms Involving Selective Interactions with
918 the Extracellular Matrix. *ISRN Inflamm.* 2013;2013: 259256. doi:10.1155/2013/259256
- 919 46. Jakubzick C V., Randolph GJ, Henson PM. Monocyte differentiation and antigen-presenting functions. *Nat Rev*
920 *Immunol.* 2017;17: 349–362. doi:10.1038/nri.2017.28
- 921 47. Perreau M, Kremer EJ. The conundrum between immunological memory to adenovirus and their use as vectors in
922 clinical gene therapy. *Mol Biotechnol.* 2006;34: 247–256. doi:10.1385/MB:34:2:247
- 923 48. Perreau M, Guérin MC, Drouet C, Kremer EJ. Interactions between human plasma components and A xenogenic
924 adenovirus vector: Reduced immunogenicity during gene transfer. *Mol Ther.* 2007;15: 1998–2007.
925 doi:10.1038/sj.mt.6300289
- 926 49. Leen AM, Christin A, Khalil M, Weiss H, Gee AP, Brenner MK, et al. Identification of Hexon-Specific CD4 and CD8
927 T-Cell Epitopes for Vaccine and Immunotherapy. *J Virol.* 2008;82: 546–554. doi:10.1128/JVI.01689-07
- 928 50. Ginder DR. Increased susceptibility of mice infected with mouse adenovirus to *Escherichia coli*-induced
929 pyelonephritis. *J Exp Med.* 1964;120: 1117–28. Available: <http://www.ncbi.nlm.nih.gov/pubmed/14238929>
- 930 51. Smith K, Brown CC, Spindler KR. The role of mouse adenovirus type 1 early region 1A in acute and persistent
931 infections in mice. *J Virol.* 1998;72: 5699–706. Available: <http://www.ncbi.nlm.nih.gov/pubmed/9621028>
- 932 52. Moore ML, McKissic EL, Brown CC, Wilkinson JE, Spindler KR. Fatal disseminated mouse adenovirus type 1
933 infection in mice lacking B cells or Bruton's tyrosine kinase. *J Virol.* 2004;78: 5584–90.
934 doi:10.1128/JVI.78.11.5584-5590.2004
- 935 53. Qureshi H, Genesca M, Fritts L, McChesney MB, Robert-Guroff M, Miller CJ. Infection with host-range mutant
936 adenovirus 5 suppresses innate immunity and induces systemic CD4+ T cell activation in rhesus macaques. *PLoS*
937 *One.* 2014;9: e106004. doi:10.1371/journal.pone.0106004
- 938 54. Berk AJ. Recent lessons in gene expression, cell cycle control, and cell biology from adenovirus. *Oncogene.* 2005.
939 pp. 7673–7685. doi:10.1038/sj.onc.1209040
- 940 55. Banchereau J, Briere F, Caux C, Davoust J, Lebecque S, Liu YJ, et al. Immunobiology of dendritic cells. *Annu Rev*

- 941 Immunol. 2000;18: 767–811.
- 942 56. von Hundelshausen P, Agten SM, Eckardt V, Blanchet X, Schmitt MM, Ippel H, et al. Chemokine interactome
943 mapping enables tailored intervention in acute and chronic inflammation. *Sci Transl Med.* 2017;9: 1–15.
944 doi:10.1126/scitranslmed.aah6650
- 945 57. Nourshargh S, Renshaw SA, Imhof BA. Reverse Migration of Neutrophils: Where, When, How, and Why? *Trends*
946 *Immunol.* 2016;37: 273–286. doi:10.1016/j.it.2016.03.006
- 947 58. Schindler R, Clark B, Dinarello C. Dissociation between interleukin-1 beta mRNA and protein synthesis in human
948 peripheral blood mononuclear cells. *J Biol Chem.* 1990;265: 10232–7.
- 949 59. Netea MG, van de Veerdonk FL, van der Meer JWM, Dinarello CA, Joosten LAB. Inflammasome-Independent
950 Regulation of IL-1-Family Cytokines. *Annu Rev Immunol.* 2015;33: 49–77. doi:10.1146/annurev-immunol-032414-
951 112306
- 952 60. Coeshott C, Ohnemus C, Pilyavskaya A, Ross S, Wieczorek M, Kroona H, et al. Converting enzyme-independent
953 release of tumor necrosis factor alpha and IL-1beta from a stimulated human monocytic cell line in the presence of
954 activated neutrophils or purified proteinase 3. *Proc Natl Acad Sci U S A.* 1999;96: 6261–6266.
955 doi:10.1073/pnas.96.11.6261
- 956 61. Cotter MJ, Zaiss AK, Muruve DA. Neutrophils interact with adenovirus vectors via Fc receptors and complement
957 receptor 1. *J Virol.* 2005;79: 14622–14631.
- 958 62. Wilson SS, Bromme BA, Holly MK, Wiens ME, Gounder AP, Sul Y, et al. Alpha-defensin-dependent enhancement
959 of enteric viral infection. *PLOS Pathog.* 2017;13: e1006446. doi:10.1371/journal.ppat.1006446
- 960 63. Menezes S, Melandri D, Anselmi G, Perchet T, Loschko J, Dubrot J, et al. The Heterogeneity of Ly6Chi Monocytes
961 Controls Their Differentiation into iNOS+ Macrophages or Monocyte-Derived Dendritic Cells. *Immunity.* 2016;45:
962 1205–1218. doi:10.1016/j.immuni.2016.12.001
- 963 64. Zhu J, Chen H, Huang X, Jiang S, Yang Y. Ly6Chi monocytes regulate T cell responses in viral hepatitis. *JCI*
964 *Insight.* 2016;1: 1–12. doi:10.1172/jci.insight.89880
- 965 65. Singh S, Vedi S, Samrat SK, Li W, Kumar R, Agrawal B. Heterologous immunity between adenoviruses and
966 hepatitis C virus: A new paradigm in HCV immunity and vaccines. *PLoS One.* 2016;11: e0146404.
967 doi:10.1371/journal.pone.0146404
- 968 66. Medzhitov R, Durieux J, Wolff S, Dillin A, Prahlad V, Cornelius T, et al. Disease tolerance as a defense strategy.
969 *Science (80-).* 2012;335: 936–941. doi:10.1126/science.1214935
- 970 67. Mynarek M, Ganzenmueller T, Mueller-Heine A, Mielke C, Gonnermann A, Beier R, et al. Patient, virus, and
971 treatment-related risk factors in pediatric adenovirus infection after stem cell transplantation: Results of a routine
972 monitoring program. *Biol Blood Marrow Transplant.* 2014;20: 250–256. doi:10.1016/j.bbmt.2013.11.009
- 973 68. Feghoul L, Chevret S, Cuinet A, Dalle JH, Ouachée M, Yacouben K, et al. Adenovirus infection and disease in
974 paediatric haematopoietic stem cell transplant patients: Clues for antiviral pre-emptive treatment. *Clin Microbiol*
975 *Infect.* 2015;21: 701–709. doi:10.1016/j.cmi.2015.03.011
- 976 69. Kremer EJ, Boutin S, Chillon M, Danos O. Canine Adenovirus Vectors: an Alternative for Adenovirus-Mediated
977 Gene Transfer. *J Virol.* 2000;74: 505–512. doi:10.1128/JVI.74.1.505-512.2000
- 978 70. Soudais C, Boutin S, Hong SS, Chillon M, Danos O, Bergelson JM, et al. Canine adenovirus type 2 attachment
979 and internalization: Coxsackievirus-adenovirus receptor, alternative receptors, and an RGD-independent pathway.
980 *J Virol.* 2000;74: 10639–10649. doi:10.1128/Jvi.74.22.10639-10649.2000
- 981 71. Imelli N, Ruzsics Z, Puntener D, Gastaldelli M, Greber UF. Genetic reconstitution of the human adenovirus type 2
982 temperature-sensitive 1 mutant defective in endosomal escape. *Virol J.* 2009/10/29. 2009;6: 174.
983 doi:10.1186/1743-422X-6-174
- 984 72. Mittereder N, Yei S, Bachurski C, Cuppoletti J, Whitsett JA, Tolstoshev P, et al. Evaluation of the efficacy and
985 safety of in vitro, adenovirus-mediated transfer of the human cystic fibrosis transmembrane conductance regulator
986 cDNA. *Hum Gene Ther.* 1994;5: 717–729.
- 987

988 **Supporting information**



989
990
991
992
993
994
995
996
997
998
999
1000
1001
1002
1003
1004
1005
1006
1007
1008

Figure S1) Transwell assay setup and controls

A) We used transwell inserts with 0.4 μm filter to generate direct and bystander DCs. Direct DCs (1.5×10^6 cells unless mentioned otherwise) were incubated with the stimulus (e.g. LPS, HAAdV5, mutant virus, \pm IVIg \pm drugs) in lower compartment for 6 h. Fresh DCs (6×10^5) were added to the upper compartment.

B) To determine if HAAdV5 particles (2×10^4 pp/ml) added to the lower chamber diffused to the upper compartment and impact the bystander DCs, we quantified (by qPCR) HAAdV5 genomes in the **supernatant** of each compartment. 1.6×10^{10} pp of HAAdV5 pp were used in the control medium. These data demonstrate that 10,000-fold fewer particles could be found in the upper chamber.

C) Quantification of HAAdV5 genomes **associated with bystander DCs** as measured by qPCR ($n \geq 3$). DNA from mock-treated samples was extracted and virus/cell was normalized to *GAPDH* copy number. The quantity of HAAdV5 genomes/cell was normalized by *lacZ* (transgene in the vector) vs. *GAPDH* copy number. While direct DCs take up ~ 600 pp/cell [14], we found that 1 in 10 bystander DC contains a single HAAdV5 genome.

D) The 7AAD⁺ bystander and direct DCs (i.e. DCs with compromised plasma membrane integrity) in each condition were quantified by flow cytometry. The assays were carried out in 4 donors (mean \pm SEM). These results demonstrate that bystander DCs do not show loss of cell membrane integrity. *p* values were derived using Student's t-test (**B & C**) or one-way ANOVA with Dunnett's post-tests (**D**). * $p < 0.05$, ** $p < 0.01$ and *** $p < 0.001$.

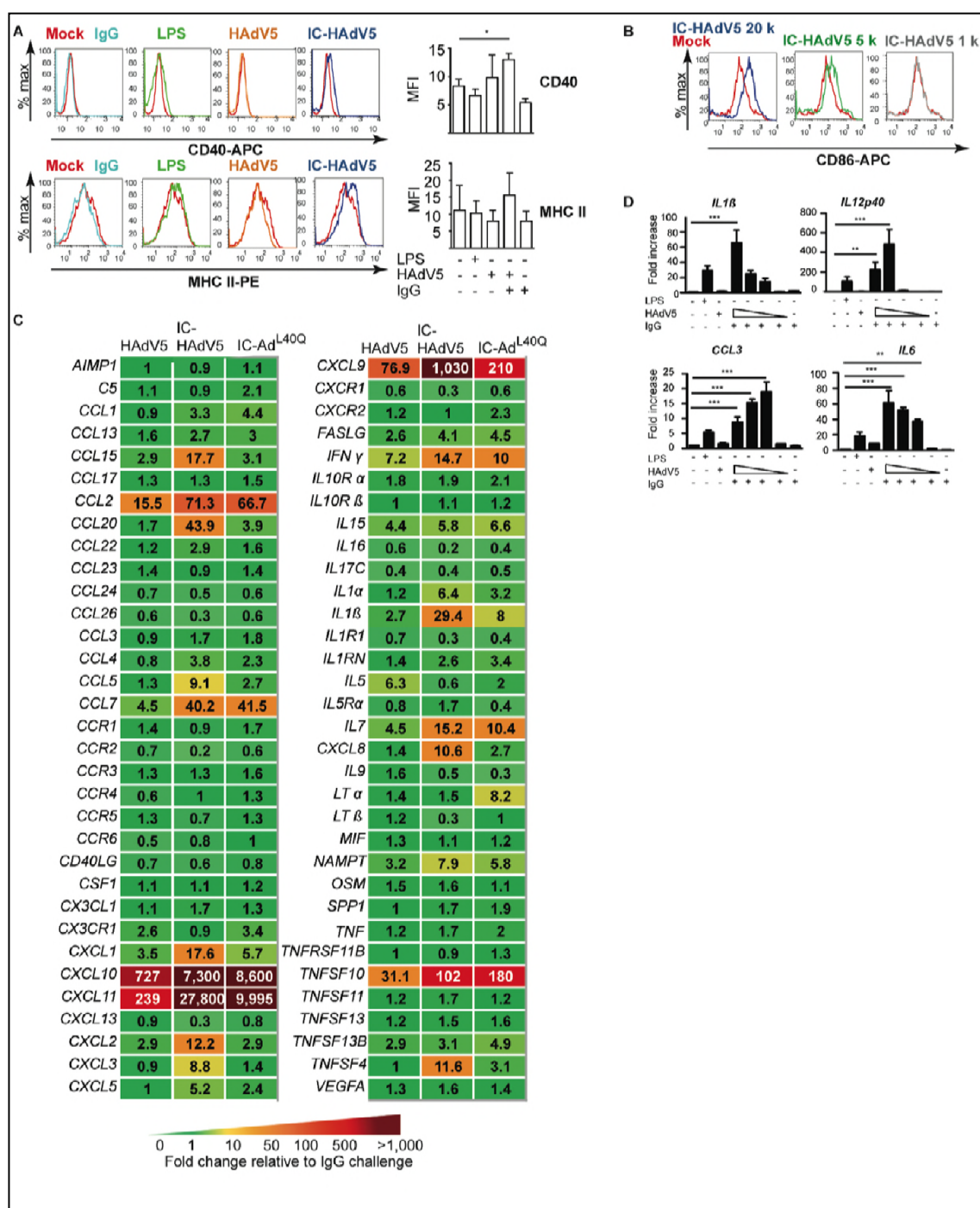


Figure S2) Maturation/activation markers on bystander DCs

Bystander DCs were generated using milieu from DCs challenged with IgG, LPS, HAdV5, or IC-HAdV5. The color code is as in **Figure 2**. **A**) The data are representative flow cytometry profiles of CD40 and MHC II surface expression. A modest increase was noted in each case. **B**) In a dose-dependent assay (20,000, 5,000, or 1,000 pp/cell) CD86 cell surface levels were quantified detected by flow cytometry. The data are representative flow cytometry profiles. Assays were carried out in 4 donors with similar results. **C**) PCR array profiles from bystander DCs exposed to the milieu generated by DCs challenged by HAdV5, IC-HAdV5, and IC-Ad^{L40Q}. The 66 cytokine mRNAs that gave unique qPCR peaks in our hands. **D**) *IL1 β* , *IL12p40*, *CCL3* and *IL6* mRNA levels in bystander THP1 DCs assayed in a dose-dependent (20,000, 10,000, 5,000, or 1,000 pp/direct DC) response. Data are mean \pm SEM with 3 independent experiments. *p* values were derived from one-way ANOVA with Dunnett's test. * *p* < 0.05, ** *p* < 0.01 and *** *p* < 0.001.

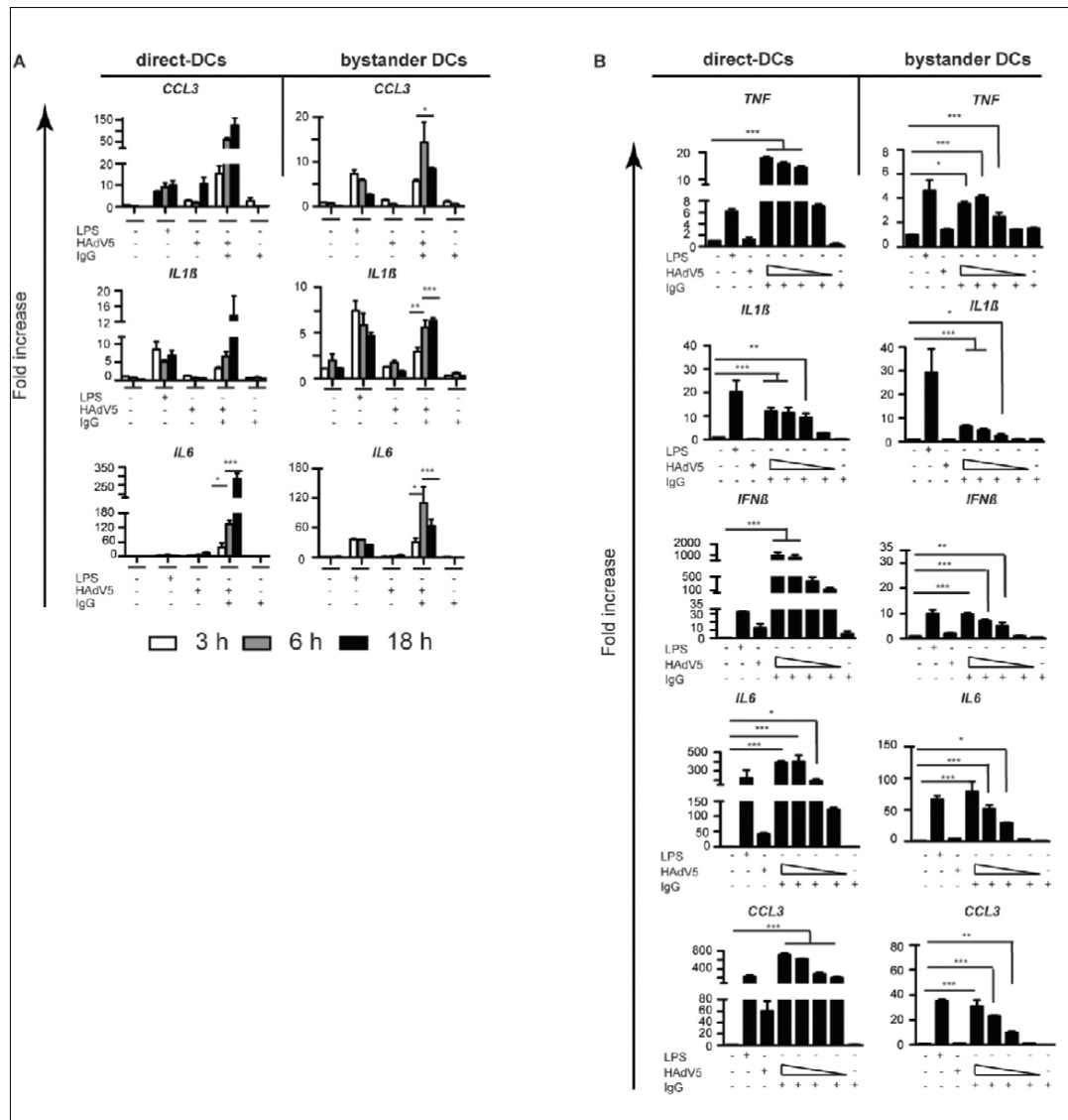


Figure S3) Bystander and direct DC cytokine mRNA levels as a function of time and dose

We extended the mRNA array results by quantifying dose-dependent responses of a handful of mRNA levels by RT-qPCR. Because DCs derived from monocytes from random blood bank donors can have widely different levels of mRNAs, we compared mRNA levels in THP-1-derived DCs to provide a standardized view of the changes. THP-1 cells were differentiated into DCs for 6 days, then directly and indirectly activated. **A)** *CCL3*, *IL1β*, and *IL6* mRNA levels in DCs challenged with LPS, IgG, HAdV5 and IC-HAdV5 (left hand column), and bystander DCs (right hand column) incubated in the respective direct DC milieu were quantified at 3, 6, and 18 h post-incubation. **B)** Changes in *TNF*, *IL1β*, *IFNβ*, *IL6*, and *CCL3* mRNA levels in direct (left hand column)

TNF: IC 2×10^4 vs. 10^4 ns; 10^4 vs. 5×10^3 ns; 5×10^3 vs. 1×10^3 ***; *IL1β* IC 2×10^4 vs. 10^4 ns; 10^4 vs. 5×10^3 ns; 5×10^3 vs. 10^3 ns; IC 2×10^4 vs. 10^3 **, IC 10^4 vs. 10^3 *;

IFNβ: IC 2×10^4 vs. 10^4 ns; 10^4 vs. 5×10^3 ns; 5×10^3 vs. 10^3 ns, IC 2×10^4 vs. 10^3 *; *IL6*: IC 2×10^4 vs. 10^4 ns; 10^4 vs. 5×10^3 **; 5×10^3 vs. 1×10^3 ns;

CCL3: IC 2×10^4 vs. 1×10^4 ns; 1×10^4 vs. 5×10^3 ***; 5×10^3 vs. 10^3 ns)

Bystander DC (right hand column) dose-dependent assay (2×10^4 , 10^4 , 5×10^3 , or 10^3 pp/cell) by RT-qPCR

TNF: IC 2×10^4 vs. 10^4 ns; 10^4 vs. 5×10^3 ns; 5×10^3 vs. 1×10^3 ns, IC 2×10^4 vs. 10^3 **, IC 10^4 vs. 10^3 ***;

IL1β: IC 2×10^4 vs. 10^4 ns; 10^4 vs. 5×10^3 ns; 5×10^3 vs. 10^3 ns;

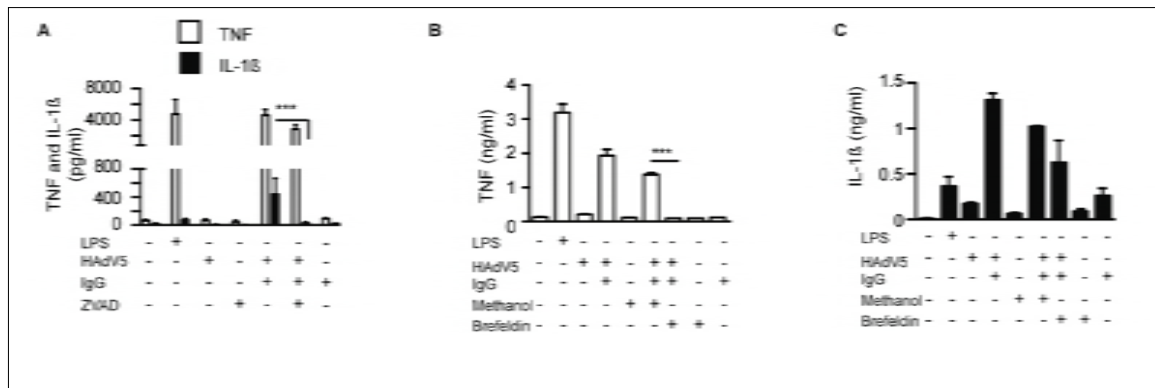
IFNβ: IC 2×10^4 vs. 10^4 ns; 10^4 vs. 5×10^3 ns; 5×10^3 vs. 10^3 ns;

IL6: IC 2×10^4 vs. 10^4 ns; 10^4 vs. 5×10^3 ns; 5×10^3 vs. 10^3 ns, 10^4 vs. 5×10^3 ***;

CCL3: IC 2×10^4 vs. 10^4 ns; 10^4 vs. 5×10^3 ***; 5×10^3 vs. 10^3 ns).

As in "A" controls included IgG and HAdV5.

Three independent experiments were carried out. Data are mean \pm SEM. *p* values were derived using Student's *t*-tests. * *p* < 0.05, ** *p* < 0.01 and *** *p* < 0.001..



1045
1046
1047
1048
1049
1050
1051
1052
1053
1054

Figure S4) Controls for ZVAD and brefeldin A assays

A) TNF and IL-1β secretion in response to ZVAD treatment (2 h before challenge) of DCs challenged with LPS, IgG, HAdV5, and IC-HAdV5.

B) DCs were simultaneously treated with brefeldin A and challenged with LPS, IgG, HAdV5, and IC-HAdV5. TNF secretion was quantified at 18 h.

C) DCs were simultaneously treated with brefeldin A and challenged with LPS, IgG, HAdV5, and IC-HAdV5. IL-1β secretion was quantified at 18 h. Data are mean ± SEM, *p* values were derived from Student's *t*-tests, *n* ≥ 3 donors. *** *p* < 0.001.

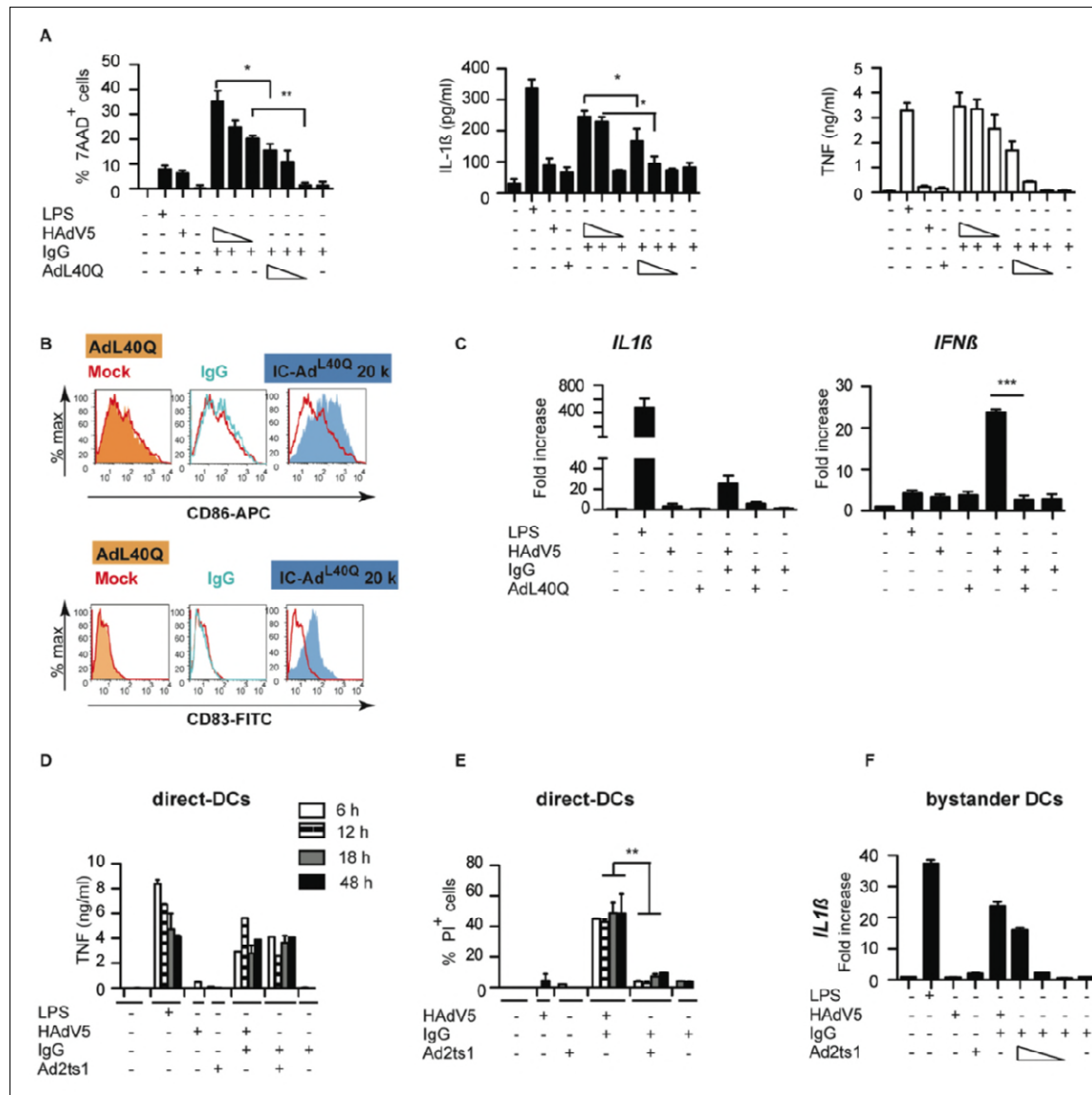


Figure S5) Controls for IC-Ad^{L40Q} and IC-Ad2ts1

A) DCs challenged with LPS, IgG, HAdV5, Ad^{L40Q} and increasing concentrations of IC-HAdV5 and IC-Ad^{L40Q} were analyzed for loss of membrane integrity (7AAD⁺ cells), IL-1 β and TNF secretion.

B) Cell surface levels of the maturation/activation markers CD86 and CD83 following direct DCs challenged with IgG, Ad^{L40Q}, IC-Ad^{L40Q}, HAdV5, and IC-HAdV5.

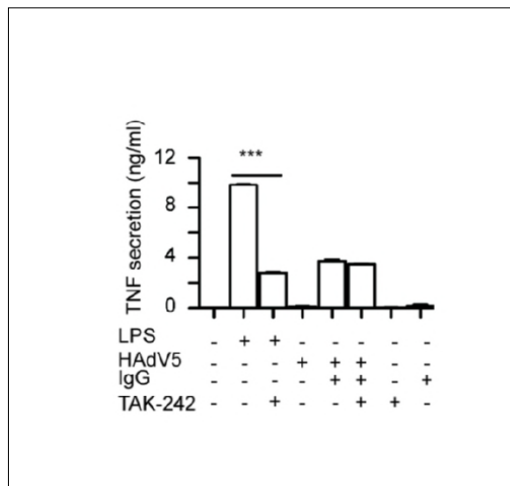
C) bystander DC *IL1 β* and *IFN β* mRNA levels quantified by RT-qPCR assay. Experiments were carried out in ≥ 3 donors. *p* values were derived from Student's *t*-tests. *, **, *** denote *p* values of < 0.05, < 0.01, < 0.001, respectively.

DCs were challenged with LPS, IgG, HAdV5, IC-HAdV5, Ad2ts1, and IC-Ad2ts1 and screened for **D)** time-dependent (6 to 48 h) TNF secretion; and **E)** time-dependent (6 to 48 h) loss of membrane integrity using propidium iodide (PI) incorporation; or

F) DCs were challenged with LPS, IgG, HAdV5, IC-HAdV5, Ad2ts1, and IC-Ad2ts1 and then used to generate bystander DCs in which the *IL1 β* mRNA levels were quantified by RT-qPCR assay following dose-dependent stimulation (20×10^3 , 10×10^3 , or 5×10^3 pp/cell) of the direct DCs.

All experiments were carried out in 3 donors and in duplicate. *P* values were derived from Student's *t*-tests. ** *p* < 0.01.

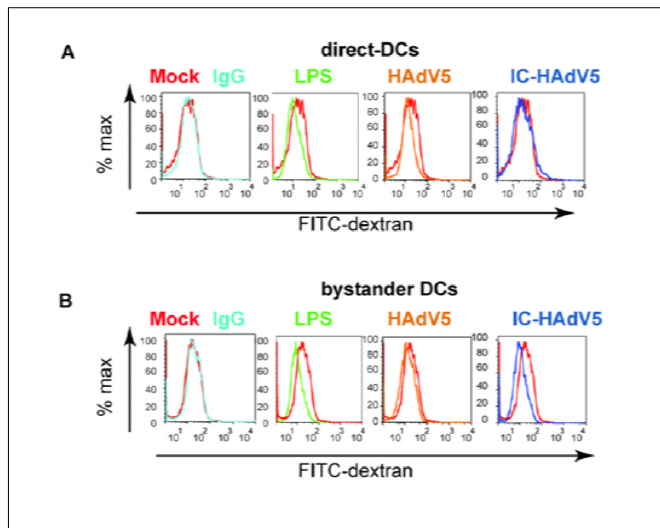
1074
1075



1076
1077
1078
1079
1080
1081

Figure S6) TAK-242 controls

Bystander DCs were treated with TAK-242 for 1 h before adding them to the DCs challenged with LPS, IgG, HAdV5, or IC-HAdV5. TNF secretion was quantified in direct DCs in the lower compartment (n = 3 donors). *p* values were derived from Student's *t*-tests. *** *p* < 0.0001.



1082
1083
1084
1085
1086
1087
1088
1089
1090

Figure S7) Controls for fluid phase uptake assay

Nonspecific binding of dextran to **A)** direct DCs and **B)** bystander DCs was controlled by incubating DC (post-stimulation) with FITC-labeled dextran at 4°C. Direct DCs were challenged with IgG, LPS, HAdV5, or IC-HAdV5. The cells were then incubated with FITC-labeled dextran and analyzed by flow cytometry. The data are representative flow cytometry profiles with experiments performed using cells from in 3 donors and in duplicate.

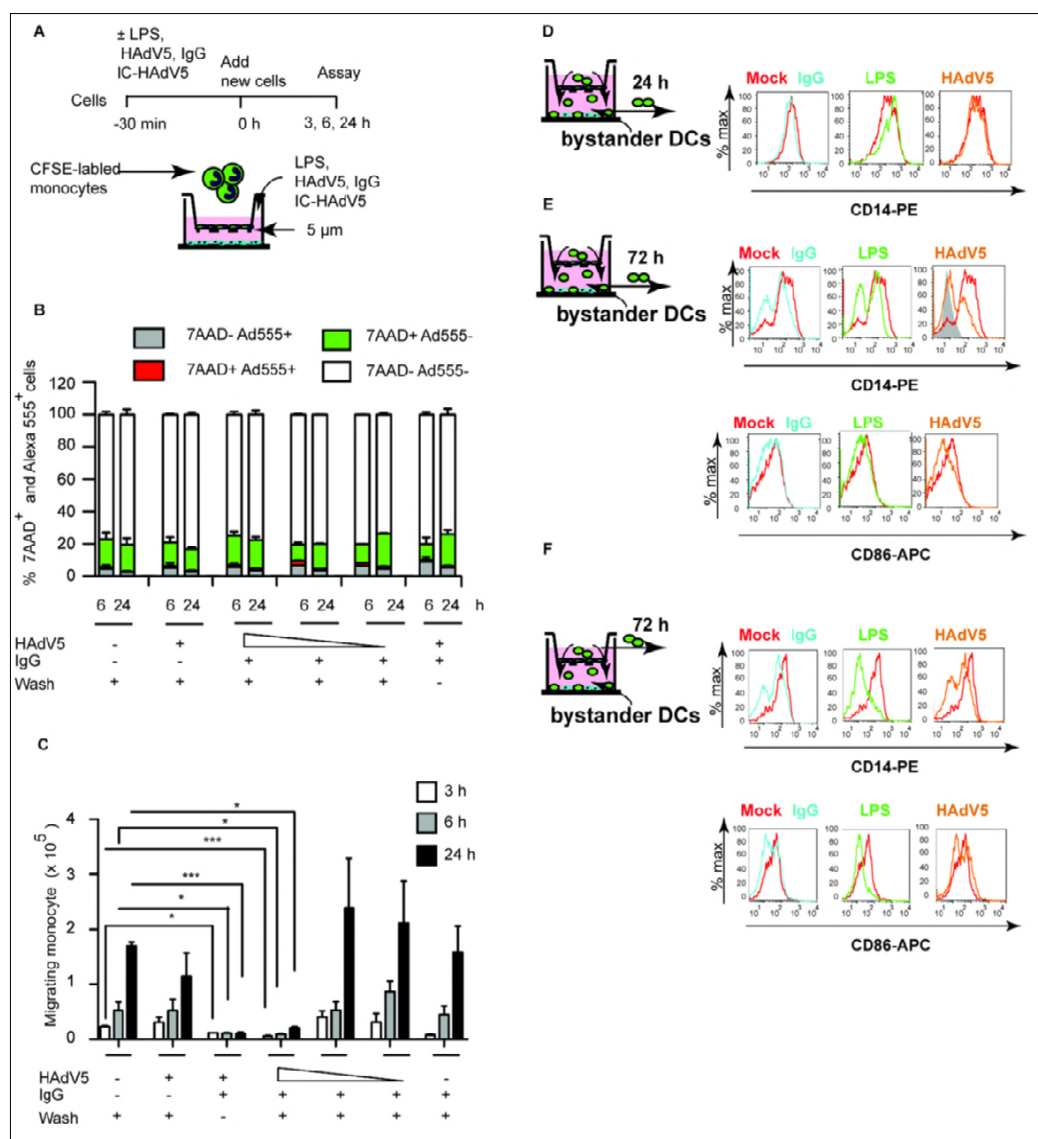
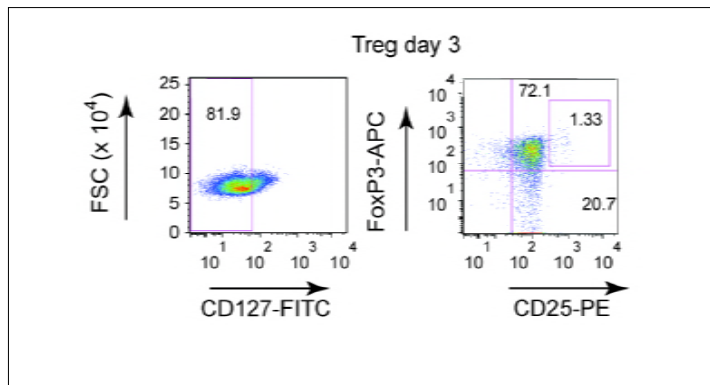


Figure S8) Controls for monocyte recruitment

A) A 5-micron-pore membrane transwell system was used for monocyte migration assays. The timing and stimuli are indicated in the schematics. Round green cells are CFSE-labeled monocytes. **B)** These data shown percentage of monocyte in the upper chamber that potentially interact with HAdV or IC-HAdV5. **C)** To address this possibility, we covalently linked Alexa555 to the HAdV5 capsid (HAdV5-Alexa555 [29]) to identify cells associated with HAdV5 or IC-HAdV5. CFSE-labeled monocytes were then assayed by flow cytometry for loss of membrane integrity (7AAD⁺ cells) and the presence of HAdV5-Alexa555 at 6 and 24 h. These data demonstrate that ICs do not go through the pore to interact with monocytes in the upper chamber. **D)** CD14 expression levels on monocytes recruited towards bystander DCs that were created with the milieu from DCs challenged with IgG, LPS or HAdV5 at 24 h. **E)** CD14 and CD86 levels on monocytes recruited to bystander DCs that were created with the milieu from DCs challenged with IgG, LPS or HAdV5 at 72 h. **F)** CD14 and CD86 expression levels on monocytes that remained in the upper compartment at 72 h. The lower compartment contained bystander DCs that were created with the milieu from DCs challenged with IgG, LPS or HAdV5. The data are representative flow cytometry profiles with assays carried out in 4 donors. * $p < 0.05$, ** $p < 0.01$ and *** $p < 0.001$.

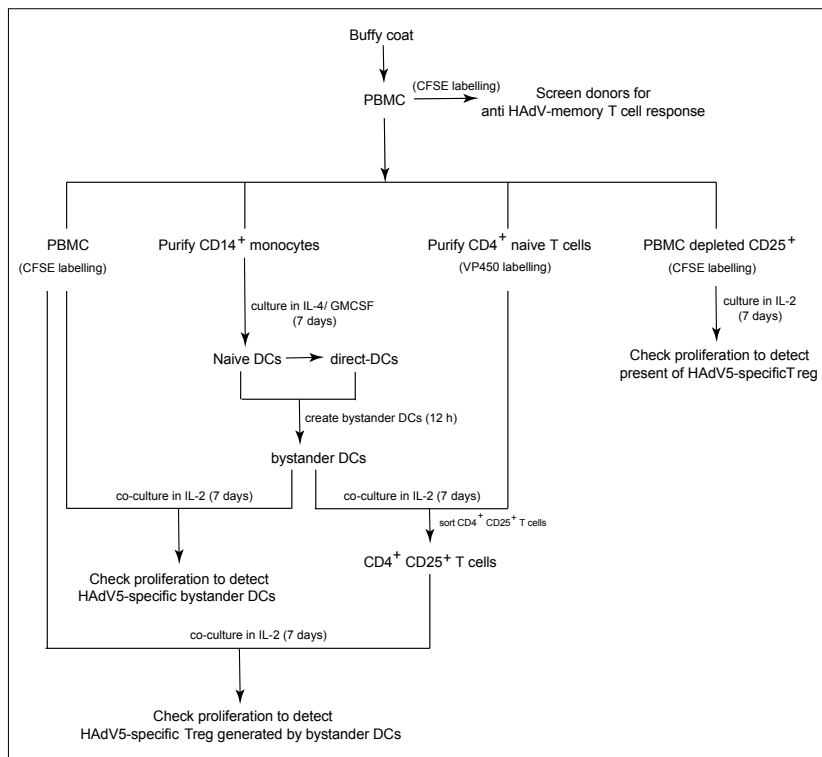
1091
1092
1093
1094
1095
1096
1097
1098
1099
1100
1101
1102
1103
1104
1105
1106



1107
1108

1109 **Figure S9)** Bystander DCs, generated using the media from DCs challenged with IgG, HAdV5, and IC-
1110 HAdV5, were incubated with naive CD4⁺ T cells isolated from the same donors. Three days post-incubation
1111 we gated on CD127^{dim} cells to identify CD25⁺/FoxP3^{high} cells. The data are representative flow cytometry
1112 profiles with assays carried out in 7 donors.

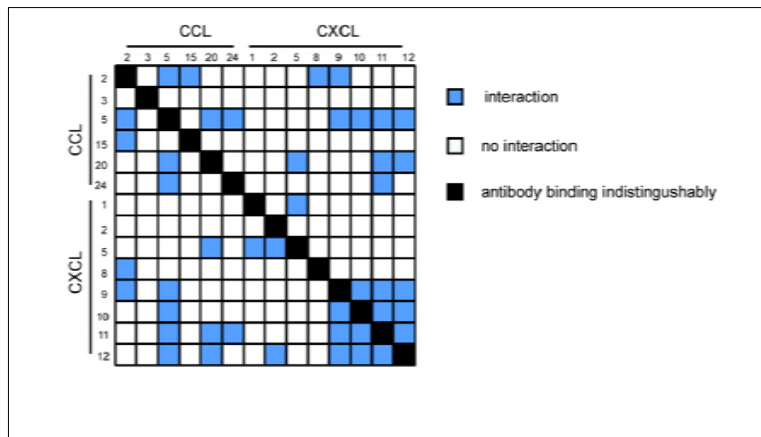
1113



1114
1115
1116

Figure S10) Flow chart demonstrating the cells and process used for the T_{reg} assays

1117
1118



1119
1120
1121
1122
1123

Figure S11) Potential cytokine heterodimer formation/interactions

Potential cytokine heterodimers are based on von Hundelshausen *et al.* [56] interactome data and the response generated by direct and bystander DCs.

1124
1125

Table S1) Statistical analyses of bystander DC cytokine transcription profile

cytokine	condition 1	condition 2	significance
TNF	IC 2 x 10 ⁴ pp/cell	IC 10 ⁴ pp/cell	p <0.0001
	IC 1 x 10 ⁴ pp/cell	IC 5 x 10 ³ pp/cell	p >0.05
	IC 5 x 10 ³ pp/cell	IC 1 x 10 ³ pp/cell	p <0.0001
IFNβ	IC 2 x 10 ⁴ pp/cell	IC 1 x 10 ⁴ pp/cell	p <0.0001
	IC 1 x 10 ⁴ pp/cell	IC 5 x 10 ³ pp/cell	p >0.05
	IC 5 x 10 ³ pp/cell	IC 1 x 10 ³ pp/cell	p <0.0001
CXCL10	IC 2 x 10 ⁴ pp/cell	IC 1 x 10 ⁴ pp/cell	p <0.0001
	IC 1 x 10 ⁴ pp/cell	IC 5 x 10 ³ pp/cell	p >0.05
	IC 5 x 10 ³ pp/cell	IC 1 x 10 ³ pp/cell	p <0.0001

1126

1127 **Table S2: In-house designed primer sequences**

Gene	Primer sequences
<i>TNF</i>	5'- CTCTGGCCCAGGCAGTCAGA -3' [forward]
	5'- GGCCTTTGGGAAGGTTGGAT -3' [reverse]
<i>IL1β</i>	5'- AACAGATGAAGTGCTCCTTCC -3' [forward]
	5'- AAGATGAAGGAAAGAAGGTGC -3' [reverse]
<i>IFNβ</i>	5'- GTCTCCTCCAAATTGCTCTC -3' [forward]
	5'- ACAGGAGCTTCTGACACTGA -3' [reverse]
<i>CXCL10</i>	5'- TATTCCTGCAAGCCAATTTTGTG -3' [forward]
	5'- TCTTGATGGCCTTCGATTCTG -3' [reverse]
<i>IL6</i>	5'- CCAGGAGCCCAGCTATGAAC -3' [forward]
	5'- CCCAGGGAGAAGGCAACTG -3' [reverse]
<i>IL12 (p40)</i>	5'- CCAAGAACTTGCAGCTGAAG -3' [forward]
	5'- TGGGTCTATTCCGTTGTGTC -3' [reverse]
<i>CCL3</i>	5'- CTGCATCACTTGCTGCTGACA -3' [forward]
	5'- CACTGGCTGCTCGTCTCAAAG -3' [reverse]
<i>GAPDH</i>	5'-ACAGTCCATGCCATCACTGCC-3' [forward]
	5'-GCCTGCTTCAACACCTTCTTG-3' [reverse]

1128